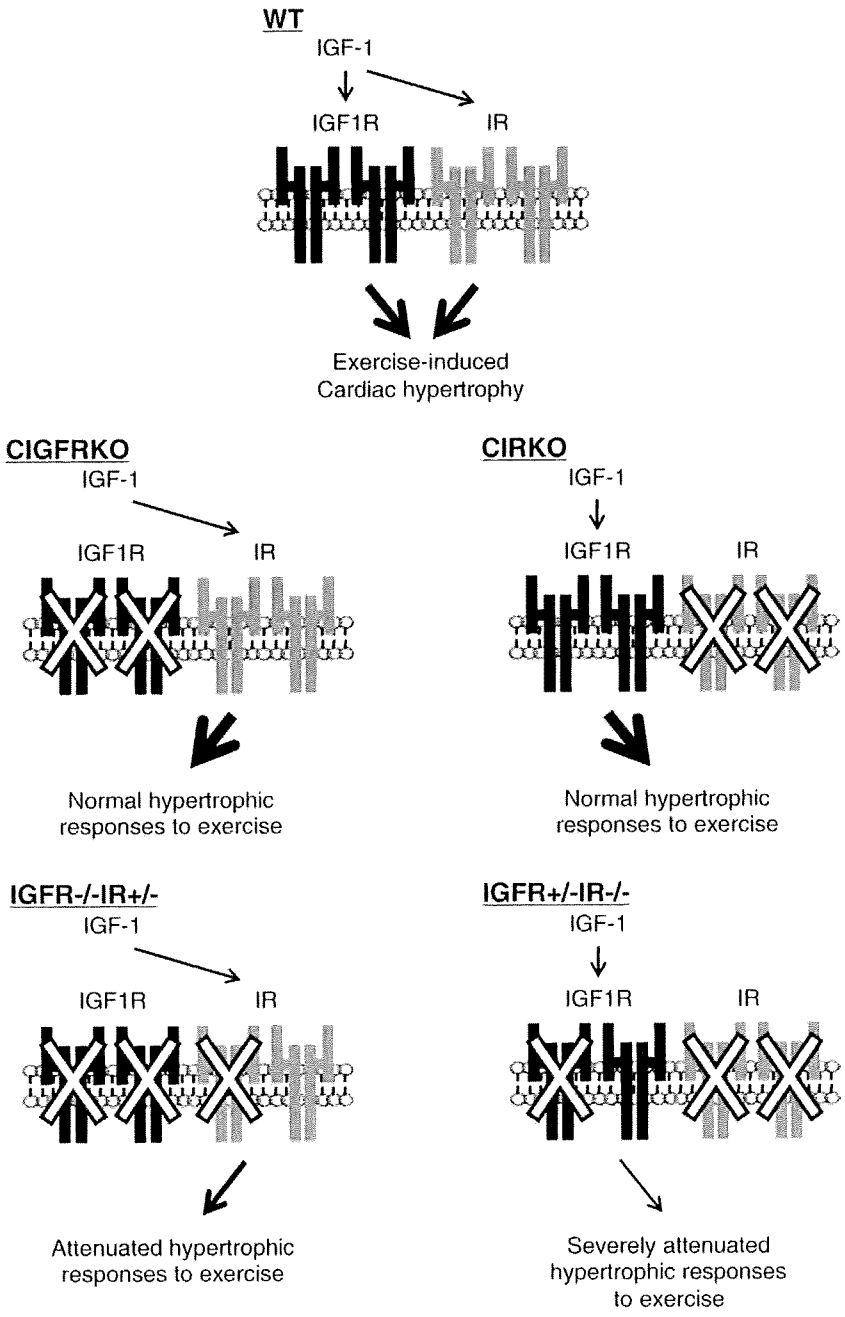

Fig. 10. Schematic illustration of the interaction and cross talk between IGF1R- and IR-mediated signals in exercise-induced cardiac hypertrophy. IGF-1 activates both IGF1R and IR in the heart in response to exercise training. Exercise-induced cardiac hypertrophy develops normally in CIGFRKO mice and CIRKO mice, although combined deletion of two *Igf1r* alleles and one *Ir* allele or one *Igf1r* allele and two *Ir* alleles results in the attenuation of exercise-induced hypertrophy. Thus, exercise-induced cardiac hypertrophy is mediated both by IGF1R- and IR-mediated signals in a redundant fashion. IGF-1 appears to be a major factor that activates both IGF1R and IR. The contribution of insulin in exercise-induced cardiac hypertrophy is not clear from our present study.

[16] McMullen JR, Shioi T, Zhang L, Tarnavski O, Sherwood MC, Kang PM, Izumo S. Phosphoinositide 3-kinase(p110alpha) plays a critical role for the induction of physiological, but not pathological, cardiac hypertrophy. Proc Natl Acad Sci U S A 2003;100:12355–60.
[17] Condorelli G, Drusco A, Stassi G, Bellacosa A, Roncarati R, Iaccarino G, Russo MA, Gu Y, Dalton N, Chung C, Latronico MV, Napoli C, Sadoshima J, Croce CM, Ross Jr J. Akt induces enhanced myocardial contractility and cell size in vivo in transgenic mice. Proc Natl Acad Sci U S A 2002;99:12333–8.
[18] Shiojima I, Sato K, Izumiya Y, Schiekofer S, Ito M, Liao R, Colucci WS, Walsh K. Disruption of coordinated cardiac hypertrophy and angiogenesis contributes to the transition to heart failure. J Clin Invest 2005;115:2108–18.
[19] DeBosch B, Treskov I, Lupu TS, Weinheimer C, Kovacs A, Courtois M, Muslin AJ. Akt1 is required for physiological cardiac growth. Circulation 2006;113: 2097–104.
[20] Kim J, Wende AR, Sena S, Theobald HA, Soto J, Sloan C, Wayment BE, Litwin SE, Holzenberger M, Leroith D, Abel ED. IGF-1 receptor signaling is required for exercise-induced cardiac hypertrophy. Mol Endocrinol 2008;22:2531–43.
[21] Belke DD, Betuing S, Tuttle MJ, Graveleau C, Young ME, Pham M, Zhang D, Cooksey RC, McClain DA, Litwin SE, Taegtmeyer H, Severson D, Kahn CR, Abel ED. Insulin signaling coordinately regulates cardiac size, metabolism, and contractile protein isoform expression. J Clin Invest 2002;109:629–39.
[22] Shiojima I, Yefremashvili M, Luo Z, Kureishi Y, Takahashi A, Tao J, Rosenzweig A, Kahn CR, Abel ED, Walsh K. Akt signaling mediates postnatal heart growth in response to insulin and nutritional status. J Biol Chem 2002;277:37670–7.
[23] Holzenberger M, Leneuve P, Hamard G, Ducos B, Perin L, Binoux M, Le Bouc Y. A targeted partial invalidation of the insulin-like growth factor I receptor gene in mice causes a postnatal growth deficit. Endocrinology 2000;141:2557–66.
[24] Abel ED, Kaulbach HC, Tian R, Hopkins JC, Duffy J, Doetschman T, Minnemann T, Boers ME, Hadro E, Oberste-Berghaus C, Quist W, Lowell BB, Ingwall JS, Kahn BB. Cardiac hypertrophy with preserved contractile function after selective deletion of GLUT4 from the heart. J Clin Invest 1999;104:1703–14.
[25] Leneuve P, Zaoui R, Monget P, Le Bouc Y, Holzenberger M. Genotyping of Cre-lox mice and detection of tissue-specific recombination by multiplex PCR. Biotechniques 2001;31:1156–60,1162.

[26] Oka T, Maillet M, Watt AJ, Schwartz RJ, Aronow BJ, Duncan SA, Molkentin JD. Cardiac-specific deletion of Gata4 reveals its requirement for hypertrophy, compensation, and myocyte viability. Circ Res 2006;98:837–45.
[27] Laustsen PG, Russell SJ, Cui L, Entingh-Pearsall A, Holzenberger M, Liao R, Kahn CR. Essential role of insulin and insulin-like growth factor 1 receptor signaling in cardiac development and function. Mol Cell Biol 2007;27:1649–64.
[28] Taniguchi CM, Emanuelli B, Kahn CR. Critical nodes in signalling pathways: insights into insulin action. Nat Rev Mol Cell Biol 2006;7:85–96.
[29] Slaaby R, Schaffer L, Lautrup-Larsen I, Andersen AS, Shaw AC, Mathiasen IS, Brandt J. Hybrid receptors formed by insulin receptor (IR) and insulin-like growth factor I receptor (IGF-IR) have low insulin and high IGF-1 affinity irrespective of the IR splice variant. J Biol Chem 2006;281:25869–74.
[30] Rother KI, Accili D. Role of insulin receptors and IGF receptors in growth and development. Pediatr Nephrol 2000;14:558–61.
[31] Denley A, Carroll JM, Brierley GV, Cosgrove L, Wallace J, Forbes B, Roberts Jr CT. Differential activation of insulin receptor substrates 1 and 2 by insulin-like growth factor-activated insulin receptors. Mol Cell Biol 2007;27:3569–77.

Journal of Molecular and Cellular Cardiology 47 (2009) 698–705

Contents lists available at ScienceDirect

Journal of Molecular and Cellular Cardiology

journal homepage: www.elsevier.com/locate/yjmcc

Original article

Chronic doxorubicin cardiotoxicity is mediated by oxidative DNA damage-ATM-p53-apoptosis pathway and attenuated by pitavastatin through the inhibition of Rac1 activity

Masashi Yoshida [a], Ichiro Shiojima [a,b], Hiroyuki Ikeda [a], Issei Komuro [a,b,*]

[a] Department of Cardiovascular Science and Medicine, Chiba University Graduate School of Medicine, 1-8-1 Inohana, Chuo-ku, Chiba, 260-8670, Japan
[b] Department of Cardiovascular Medicine, Osaka University Graduate School of Medicine, 2-2 Yamadaoka, Suita 565-0871, Japan

ARTICLE INFO

Article history:
Received 20 May 2009
Received in revised form 8 July 2009
Accepted 27 July 2009
Available online 3 August 2009

Keywords:
Doxorubicin
Cardiomyopathy
p53
Apoptosis
Statins

ABSTRACT

Doxorubicin is known to have cumulative dose-dependent cardiotoxicity, and a tumor suppressor protein p53 has been implicated in the pathogenesis of doxorubicin cardiotoxicity. However, how p53 is induced by doxorubicin and mediates the cardiotoxic effects of doxorubicin remains elusive. In cultured cardiac myocytes, doxorubicin induced oxidative stress, DNA damage, ATM activation, and p53 induction. A free radical scavenger NAC attenuated all of these events, whereas an ATM kinase inhibitor wortmannin attenuated doxorubicin-induced ATM activation and p53 induction but not oxidative stress. Doxorubicin treatment in vivo also induced oxidative stress, DNA damage, ATM activation, and p53 accumulation. These observations suggest that p53 induction by doxorubicin is mediated by oxidative DNA damage-ATM pathway. Doxorubicin-induced contractile dysfunction and myocyte apoptosis in vivo were attenuated in heterozygous p53 deficient mice and cardiac-restricted Bcl-2 transgenic mice, suggesting that myocyte apoptosis plays a central role downstream of p53 in doxorubicin cardiotoxicity. We also tested whether pitavastatin exerts protective effects on doxorubicin cardiotoxicity. Pitavastatin attenuated doxorubicin-induced oxidative stress, DNA damage, ATM activation, p53 accumulation, and apoptosis in vitro. Pitavastatin also attenuated myocyte apoptosis and contractile dysfunction in vivo. The beneficial effects of pitavastatin were reversed by intermediate products of the mevalonate pathway that are required for the activation of Rac1, and Rac1 inhibitor exhibited cardioprotective effects comparable to those of pitavastatin. These data collectively suggest that doxorubicin-induced cardiotoxicity is mediated by oxidative DNA damage-ATM-p53-apoptosis pathway, and is attenuated by pitavastatin through its antioxidant effect involving Rac1 inhibition.

1. Introduction

Doxorubicin is a potent chemotherapeutic agent used for a wide variety of malignancies. However, the use of doxorubicin is limited due to its cumulative dose-dependent cardiotoxicity, which sometimes results in doxorubicin cardiomyopathy [1,2]. Although the precise mechanism of doxorubicin-induced cardiotoxicity is not completely understood, oxidative stress has been proposed as one of the mechanisms of cardiotoxicity by doxorubicin. Acute or chronic doxorubicin cardiotoxicity is reduced in transgenic mice overexpressing mitochondrial MnSOD or cysteine-rich metallothioneins, respectively [3,4], supporting the idea that oxidative stress mediates doxorubicin cardiotoxicity. It has also been suggested that a tumor suppressor protein p53 is a critical mediator of doxorubicin cardiotoxicity. This notion is supported by the observation that doxorubicin induces p53 accumulation in the heart and that either pharmacological or genetic ablation of p53 results in the attenuation of cardiotoxicity following doxorubicin treatment [5,6]. However, how p53 is activated in the heart by doxorubicin or how p53 mediates the cardiotoxic effects of doxorubicin remains elusive. Although myocyte apoptosis induced by doxorubicin was attenuated by p53 ablation [5,6], this does not directly demonstrate the causative role of cardiomyocyte apoptosis in doxorubicin-mediated cardiotoxicity. It was recently shown that p53 inhibits hypoxia-inducible factor-1 (Hif-1) and thereby promotes myocardial ischemia [7]. More recently, p53-dependent inhibition of mammalian target of rapamycin (mTOR) was proposed as a mechanism of acute doxorubicin cardiotoxicity independently of p53-induced apoptosis [8]. Thus, it is possible that p53-dependent but apoptosis-independent mechanisms also contribute to the pathogenesis of doxorubicin cardiotoxicity.

The 3-hydroxy-3-methylglutaryl-CoA (HMG-CoA) reductase inhibitors or statins are widely used as a cholesterol lowering drug, and also known to be cardioprotective through lipid lowering-independent pleiotropic effects [9]. For instance, statin treatment protects against

* Corresponding author. Department of Cardiovascular Science and Medicine, Chiba University Graduate School of Medicine, 1-8-1 Inohana, Chuo-ku, Chiba, 260-8670, Japan.
E-mail address: komuro-tky@umin.ac.jp (I. Komuro).

0022-2828/$ – see front matter © 2009 Elsevier Inc. All rights reserved.
doi:10.1016/j.yjmcc.2009.07.024

stroke, ischemia–reperfusion injury, cardiac hypertrophy, and heart failure in normocholesterolemic animals [10–13]. Most of these pleiotropic effects are thought to be mediated by inhibiting the synthesis of isoprenoid intermediates such as farnesyl pyrophosphate (FPP) and geranylgeranyl pyrophosphate (GGPP) downstream of the mevalonate pathway [9]. FPP and GGPP serve as lipid attachments for the post-translational modifications of a variety of proteins including small G proteins. Of note, activation of NADPH oxidase requires geranylgeranylation of Rac1 [14], and it was shown that the protective effect of statins against cardiac hypertrophy is mediated by its antioxidant effects involving the inhibition of Rac1 activity [12]. Whether statins exert protective effects against doxorubicin cardiotoxicity by similar mechanisms remains unknown.

In this study we explored how p53 accumulation is induced by doxorubicin and how p53 mediates the cardiotoxic effects of doxorubicin. We also examined the potential mechanisms of cardioprotection by statins against doxorubicin. We show that doxorubicin cardiotoxicity is mediated by oxidative DNA damage-ATM-p53-apoptosis pathway and attenuated by pitavastatin through the inhibition of Rac1 activity.

2. Materials and methods

2.1. Reagents

Doxorubicin was from Kyowa Hakko Kogyo (Tokyo, Japan). N-acetyl-L-cysteine (NAC), mevalonolactone, farnesyl pyrophosphate (FPP), geranylgeranyl pyrophosphate (GGPP), NADPH, and lucigenin were from Sigma (St. Louis, Missouri). Wortmannin, farnesyltransferase inhibitor (FTI (FTI-276)), geranylgeranyl transferase inhibitor (GTI (GTI-286)), Rac1 inhibitor (NSC23766), and apocynin were from Calbiochem (San Diego, California). Dihydroethidium (DHE) and 5-(and-6)-chloromethyl-2′, 7′-dichlorodihydrofluorescein diacetate, acetyl ester (CM-H2DCFDA) were from Molecular Probes (Eugene, Oregon). Hydrogen peroxide (H_2O_2) was from Wako (Osaka, Japan). Pitavastatin was provided by Kowa (Tokyo, Japan).

2.2. Cell culture and treatment

Neonatal rat cardiomyocytes were prepared as previously described [15]. Doxorubicin (1 μM) was added to culture media 24 h after myocyte preparation. Where indicated, cells were pretreated for 30 min with the following compounds: wortmannin, 1–50 μM; NAC, 1–50 μM; pitavastatin, 0.1–10 μM; mevalonate, 200 μM; GGPP, 10 μM; FPP, 10 μM; GTI, 30 μM; FTI, 20 nM; Rac1 inhibitor, 100 μM.

2.3. Animal models

C57BL/6 mice were purchased from SLC (Shizuoka, Japan). Heterozygous p53 deficient mice on C57BL/6 background were from Jackson Laboratory (Bar Harbar, Maine). For experiments using p53 heterozygous knockout mice, C57BL/6 mice were used as controls. Generation and genotyping of transgenic mice with cardiac-restricted overexpression of human Bcl-2 have been previously described [16]. Bcl-2 transgenic mice were on mixed background and their non-transgenic littermates were used as controls. Doxorubicin treatment was performed with intraperitoneal injection of doxorubicin (6 mg/kg) once a week for 4 weeks. Pitavastatin (3 mg/kg) treatment was performed with daily oral administration. All animal procedures were performed with the approval of the Institutional Animal Care and Use Committee of Chiba University.

2.4. Echocardiography

Transthoracic echocardiography was performed with Vevo 660 (VISUAL SONIC, Ontario, Canada) equipped with a 25-MHz imaging transducer. All recordings were performed on conscious animals.

2.5. Oxidative stress detection

Total intracellular oxidation in cultured cardiomyocytes was assessed with 2′, 7′-dichlorofluorescein (DCF) fluorescence using CM-H2DCFDA. Intracellular oxidative stress was monitored by microscopic observation and measurement of intracellular fluorescence intensity using the Mithras LB940 (Berthold, Germany) as previously described [17]. Measurements were carried out for 5 samples in each group according to the manufacturer's instruction. Histological detection of superoxide production was assessed with DHE as previously described [18].

2.6. DNA damage detection

To assess DNA damage in cultured cardiomyocytes, CometAssay (Trevigen, Gaithersburg, MD, USA) was performed according to the manufacturer's instruction. During electrophoresis, undamaged DNA remains within the confines of the nucleus, whereas damaged DNA migrates out of the nucleus in the shape of a comet. Each comet was assigned a value of 0 (no tail) to 4 (almost all DNA in tail), and 100 cells per slide and 3 slides per treatment were analyzed. To assess DNA damage in the heart in vivo, paraffin sections of the heart samples fixed in 10% formalin were stained with an antibody against phosphorylated histone H2AX (γH2AX) (Cell Signaling Technology, Beverly, Massachusetts) and dystrophin (Novocastra Laboratories, Newcastle, UK).

2.7. Western blot analysis

Western blot analysis was performed as previously described [7]. Unless mentioned otherwise, whole cell or tissue lysates were used for analysis. For Rac1 subcellular localization assay, membrane and cytosolic proteins were prepared using proteoextract native membrane protein extraction kit (Calbiochem) according to the manufacturer's instruction. Specific signals were detected using enhanced chemiluminescence (Amersham, Buckinghamshire, UK). The primary antibodies used for western blotting were as follows: phospho-ATM (S1981) (Rockland, Philadelphia, Pennsylvania), ATM (Santa Cruz Biotechnology), phospho-p53 (S15) (Santa Cruz Biotechnology), p53 (Cell Signaling Technology), Bax (Santa Cruz Biotechnology), cleaved caspase-3 (Cell Signaling Technology), Rac1 (Santa Cruz Biotechnology), and actin (Sigma).

2.8. NADPH oxidase assay

NADPH oxidase activity was measured as previously described [19]. All measurements were performed as triplicates in 96-well luminometer plates.

2.9. Cell death assay

The number of viable cells in vitro was determined with trypan blue exclusion method [20]. For apoptosis analysis in vitro and in vivo, TUNEL labeling was performed according to the manufacturer's protocol (In Situ Apoptosis Detection Kit; Takara, Shiga, Japan). TUNEL-positive cells were counted in 3 randomly selected low-power fields from each culture dish, 3 dishes for each group in vitro. TUNEL/dystrophin double positive cells were counted in 20 randomly selected high-power fields from each heart sample in vivo.

2.10. Statistical analysis

All values are expressed as means ± SEM. Multiple group comparison was performed by one-way ANOVA followed by the Tukey's HSD for comparison of means. Comparisons between two groups were analyzed by two-way ANOVA. Data processing and analysis were performed by using JMP version 5.1 (Statical Analysis

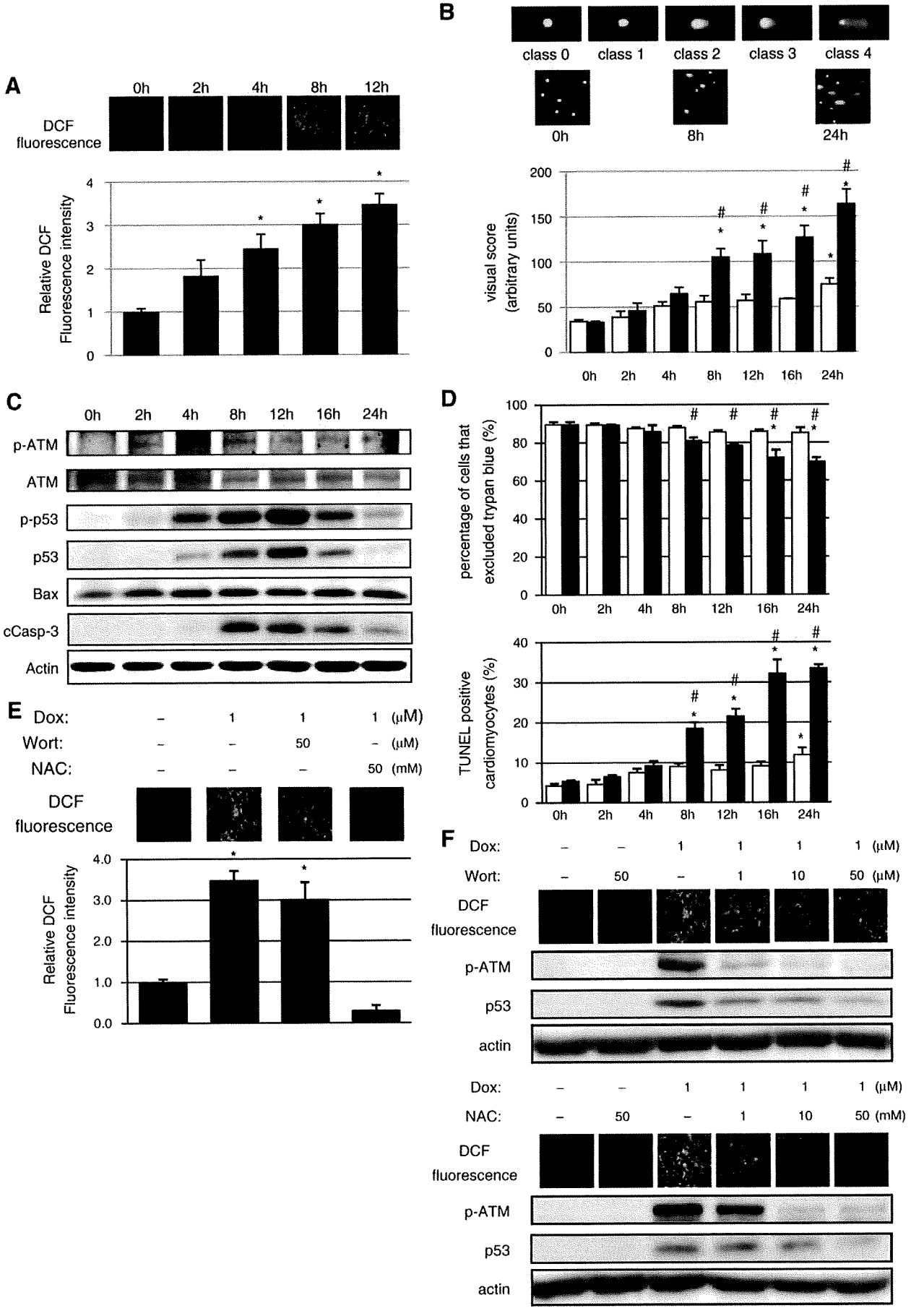
A
0h
2h
4h
8h
12h
DCF fluorescence
Relative DCF Fluorescence intensity
B
class 0
class 1
class 2
class 3
class 4
0h
8h
24h
visual score (arbitrary units)
0h 2h 4h 8h 12h 16h 24h
C
0h 2h 4h 8h 12h 16h 24h
p-ATM
ATM
p-p53
p53
Bax
cCasp-3
Actin
D
percentage of cells that excluded trypan blue (%)
TUNEL positive cardiomyocytes (%)
0h 2h 4h 8h 12h 16h 24h
E
Dox: – 1 1 1 (μM)
Wort: – – 50 – (μM)
NAC: – – – 50 (mM)
DCF fluorescence
Relative DCF Fluorescence intensity
F
Dox: – – 1 1 1 1 (μM)
Wort: – 50 – 1 10 50 (μM)
DCF fluorescence
p-ATM
p53
actin
Dox: – – 1 1 1 1 (μM)
NAC: – 50 – 1 10 50 (mM)
DCF fluorescence
p-ATM
p53
actin

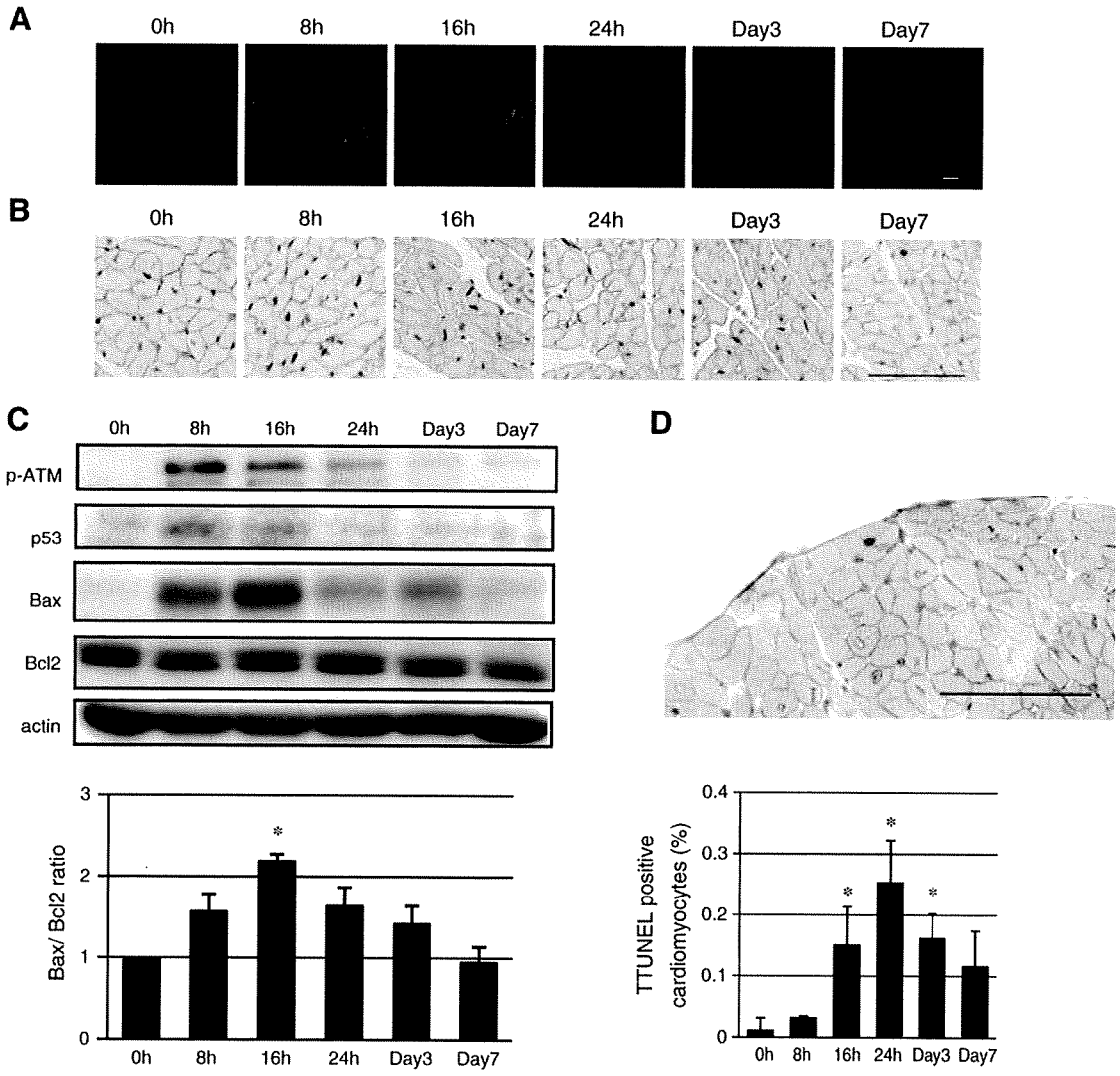

Fig. 2. Doxorubicin induces oxidative DNA damage, ATM kinase activation, and p53 accumulation in the heart in vivo. (A) Doxorubicin-induced oxidative stress in vivo. Oxidative stress was assessed by DHE assay. (B) Doxorubicin-induced DNA damage in vivo. DNA damage was assessed by γH2AX staining. (C) Doxorubicin-induced ATM activation, p53 accumulation, and cardiomyocyte apoptosis in vivo. Left: Western blot analysis. Molecular weight of Bcl2 is 26 kDa. Right: quantification of Bax/Bcl2 ratio. *P<0.05 vs 0 h. (D) Doxorubicin-induced cardiomyocyte apoptosis as assessed by TUNEL staining. Left: double-immunostaining for TUNEL (brown) and dystrophin (red) in the heart after doxorubicin treatment. Scale bar, 100 μm. Right: time course of the number of TUNEL-positive cardiomyocytes. *P<0.05 vs 0 h.

Systems). Values of P<0.05 were considered to be statistically significant.

3. Results

3.1. Doxorubicin induces p53 accumulation in cardiac myocytes via oxidative DNA damage-ATM pathway

Previous studies implicated oxidative stress and p53 accumulation in doxorubicin cardiotoxicity [1,2]. Because DNA damage links oxidative stress to p53 accumulation [21,22], we tested whether DNA damage response mediates doxorubicin cardiotoxicity in cultured cardiac myocytes. Doxorubicin treatment induced oxidative stress and DNA damage in cardiac myocytes, as assessed by DCF fluorescence and CometAssay. Statistically significant increase in DCF fluorescence and DNA damage was observed from 4 h and 8 h after doxorubicin treatment, respectively (Figs. 1(A) and (B)). Increased oxidative stress and DNA damage was associated with an increase in phospho-ATM (ataxia telangiectasia mutated) levels, p53 accumulation, and

Fig. 1. Doxorubicin induces p53 accumulation in cardiac myocytes through oxidative DNA damage-ATM pathway. (A) Doxorubicin-induced oxidative stress. Top: DCF fluorescence. Bottom: quantification of DCF fluorescence. *P<0.05 vs 0 h. (B) Doxorubicin-induced DNA damage as assessed by CometAssay. Top: classification of comets from 0 (no tail) to 4 (almost all DNA in tail). Middle: representative pictures of CometAssay at indicated time points. Bottom: time course of visual scores. White columns and black columns represent control (saline-treated) group and doxorubicin-treated group, respectively. *P<0.05 vs control group at 0 h; #P<0.05 vs control group at the same time points. (C) Doxorubicin-induced ATM activation, p53 accumulation, and cardiomyocyte apoptosis as assessed by Western blot analysis. cCasp-3, cleaved caspase-3. Molecular weights of the proteins are 370 kDa for pATM/ATM, 53 kDa for p-p53/p53, 23 kDa for Bax, 19 kDa for cleaved caspase-3, and 42 kDa for actin. (D) Doxorubicin-induced cardiomyocyte death. Top: trypan blue exclusion assay. White columns and black columns represent control (saline-treated) group and doxorubicin-treated group, respectively. *P<0.05 vs control group at 0 h; #P<0.05 vs control group at the same time points. Bottom: TUNEL assay. White columns and black columns represent control (saline-treated) group and doxorubicin-treated group, respectively. *P<0.05 vs control group at 0 h; #P<0.05 vs control group at the same time points. (E) NAC but not wortmannin attenuates doxorubicin-induced oxidative stress. Top: DCF fluorescence. Bottom: quantification of DCF fluorescence. *P<0.05 vs 0 h. (F) Both NAC and wortmannin attenuates doxorubicin-induced ATM activation and p53 accumulation. DCF fluorescence, ATM, and phospho-p53 were assessed 12 h, 4 h, and 12 h after doxorubicin treatment, respectively. Wort, wortmannin.

apoptotic cell death (Figs. 1(C) and (D)). Definitive increases in phospho-ATM and phospho-p53 were observed from 4 h after doxorubicin treatment, followed by cleaved Caspase-3 expression and apoptotic cell death from 8 h after doxorubicin treatment. This is consistent with the notion that p53 phosphorylation by ATM results in p53 stabilization, leading to apoptotic cell death. Doxorubicin-induced oxidative stress was attenuated by a free radical scavenger NAC but not by an ATM kinase inhibitor wortmannin, whereas doxorubicin-induced p53 accumulation was reduced both by NAC and wortmannin (Figs. 1(E) and (F)), indicating that ATM is situated downstream of oxidative stress in doxorubicin-induced p53 accumulation. We also checked the involvement of oxidative DNA damage-ATM pathway in doxorubicin cardiotoxicity in vivo. Single intra-peritoneal injection of doxorubicin (6 mg/kg) induced oxidative stress and DNA damage as assessed by DHE assay and γH2AX staining, respectively (Figs. 2(A) and (B)). Doxorubicin-induced oxidative stress and DNA damage in the heart were associated with a transient increase in

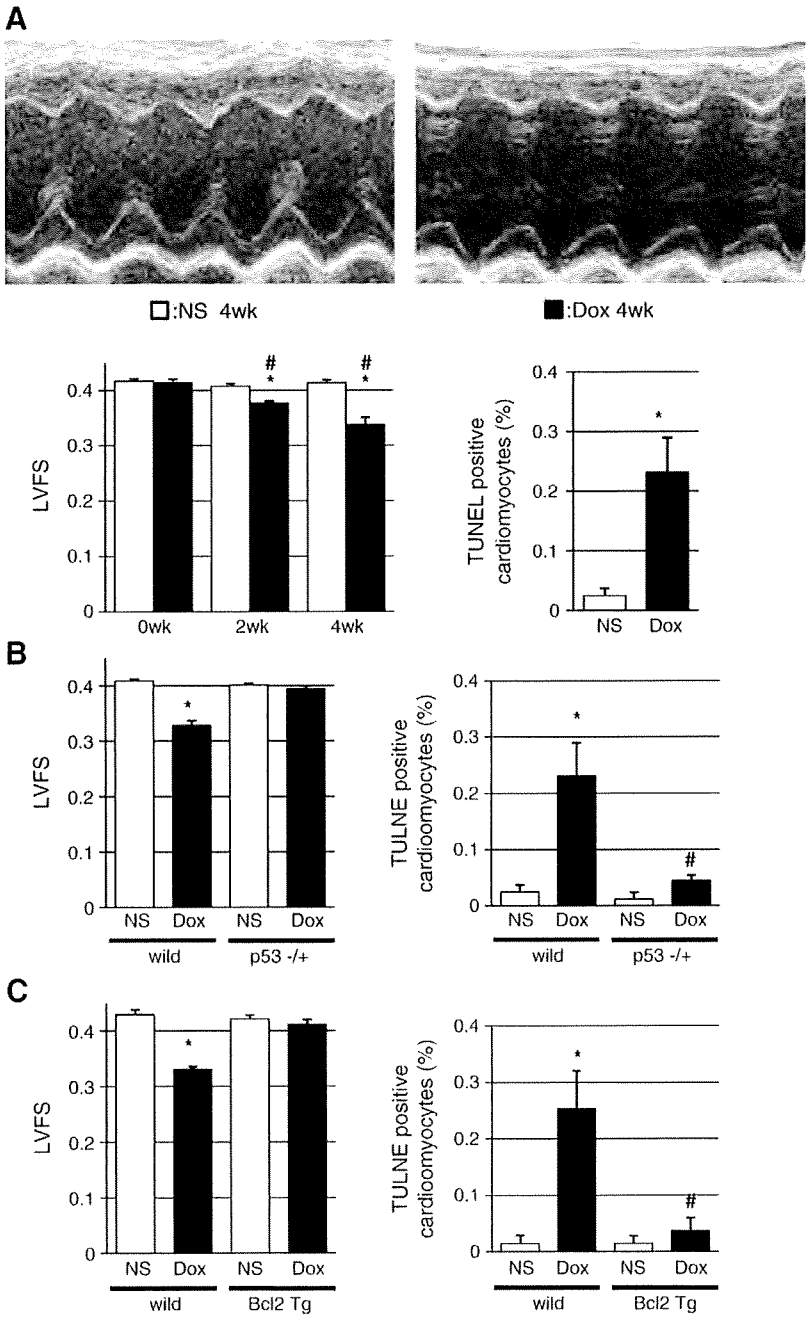

Fig. 3. Doxorubicin cardiotoxicity is mediated by p53-dependent cardiomyocyte apoptosis. (A) Doxorubicin-induced cardiomyopathy in wild type mice. Top: representative echocardiograms of the heart treated with normal saline (NS) or doxorubicin (Dox: 6 mg/kg) once a week for 4 weeks. Bottom left: left ventricular fractional shortening of mice treated with normal saline (white columns) or doxorubicin (black columns). *$P<0.05$ vs 0 week; #$P<0.05$ vs normal saline-treated group at the same time point. Bottom right: number of TUNEL-positive cardiomyocytes 4 weeks after doxorubicin treatment. *$P<0.05$ vs normal saline (NS)-treated group. (B) Doxorubicin-induced cardiomyopathy is attenuated in heterozygous p53 deficient mice. Left: left ventricular fractional shortening of mice treated with normal saline (NS) or doxorubicin (Dox). Right: number of TUNEL-positive cardiomyocytes 4 weeks after doxorubicin treatment. *$P<0.05$ vs saline-treated wild type mice; #$P<0.05$ vs doxorubicin-treated wild type mice. (C) Doxorubicin-induced cardiomyopathy is attenuated in cardiac-specific Bcl-2 transgenic mice. Left: left ventricular fractional shortening of mice treated with normal saline (NS) or doxorubicin (Dox). Right: number of TUNEL-positive cardiomyocytes 4 weeks after doxorubicin treatment. *$P<0.05$ vs saline-treated wild type mice; #$P<0.05$ vs doxorubicin-treated wild type mice.

phospho-ATM levels, p53 accumulation (Fig. 2(C)), and apoptotic cell death of myocytes as assessed by Bax/Bcl2 ratio and the number of TUNEL-positive cells (Figs. 2(C) and (D)). These data collectively suggest that doxorubicin treatment induces p53 accumulation via oxidative DNA damage-ATM pathway in cardiac myocytes.

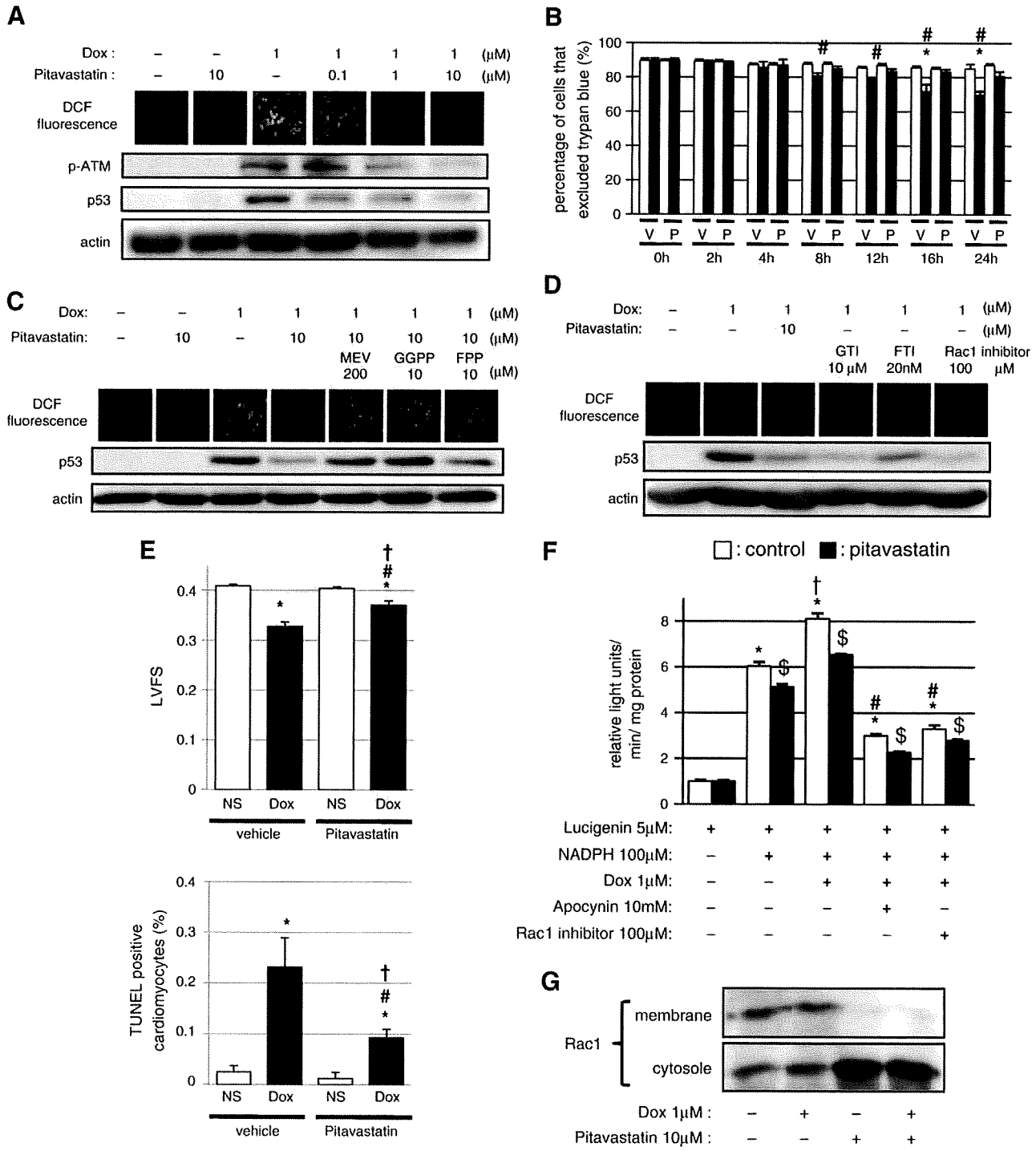

Fig. 4. Pitavastatin attenuates doxorubicin cardiotoxicity through its antioxidant effect involving Rac1 inhibition. (A) Pitavastatin attenuates doxorubicin-induced oxidative stress, ATM activation, and p53 accumulation in vitro. Oxidative stress was assessed by DCF fluorescence, and ATM activation and p53 accumulation were assessed by Western blot analysis. (B) Pitavastatin attenuates doxorubicin-induced myocyte death as assessed by trypan blue exclusion assay. White columns and black columns represent control (saline-treated) group and doxorubicin-treated group, and V and P represent vehicle and pitavastatin treatment, respectively. $^{\#}P<0.05$ vs vehicle-treated control group at the same time points; $^{*}P<0.05$ vs pitavastatin-treated doxorubicin group at the same time points. (C) Intermediate products of the mevalonate pathway reverse the beneficial effects of pitavastatin on doxorubicin cardiotoxicity. MEV, mevalonate. (D) GTI and Rac1 inhibitor but not FTI exhibit protective effects on doxorubicin cardiotoxicity. (E) Pitavastatin attenuates doxorubicin-induced cardiomyopathy. Top: left ventricular fractional shortening of mice treated with normal saline (NS) or doxorubicin (Dox). Mice were further divided into vehicle-treated group or pitavastatin-treated group. Bottom: number of TUNEL-positive cardiomyocytes 4 weeks after doxorubicin treatment. $^{*}P<0.05$ vs saline/vehicle-treated group; $^{\#}P<0.05$ vs saline/pitavastatin-treated group; $^{\dagger}P<0.05$ vs doxorubicin/vehicle-treated group. (F) Pitavastatin attenuates NADPH oxidase activity. White columns and black columns represent control (saline-treated) group and pitavastatin-treated group, respectively. $^{*}P<0.05$ vs lucigenin-treated control group; $^{\dagger}P<0.05$ vs lucigenin/NADPH-treated control group; $^{\#}P<0.05$ vs lucigenin/NADPH/doxorubicin-treated control group; $^{\$}P<0.05$ vs control group with the same treatment. (G) Pitavastatin inhibits translocation of Rac1 to plasma membrane. Molecular weight of Rac1 is 22 kDa.

3.2. Doxorubicin cardiotoxicity is mediated by p53-dependent cardiomyocyte apoptosis

We next examined the role of p53-dependent cardiomyocyte apoptosis in doxorubicin-induced cardiotoxicity in vivo. After chronic doxorubicin treatment, contractile function was impaired and apoptotic cardiomyocyte death was increased compared with vehicle treatment group in wild type mice (Fig. 3(A)). The deleterious effects of doxorubicin were attenuated in p53 heterozygous knockout mice, suggesting that p53 accumulation plays a causal role in doxorubicin cardiotoxicity (Fig. 3(B)). p53-induced cardiomyocyte apoptosis, myocardial ischemia, and mTOR inhibition have been implicated in the pathogenesis of various forms of heart failure [1,2,7,8]. However, doxorubicin cardiotoxicity was attenuated by cardiac-specific overexpression of anti-apoptotic protein Bcl-2 (Fig. 3(C)), whereas myocardial vessel density or myocyte size was not altered by chronic doxorubicin treatment (data not shown). Thus, doxorubicin cardiotoxicity is mediated by p53-dependent cardiomyocyte apoptosis.

3.3. Pitavastatin attenuates doxorubicin cardiotoxicity through its antioxidant effect involving Rac1 inhibition

Because oxidative stress is a critical inducer of p53 accumulation in the heart by doxorubicin and statins have been shown to have antioxidant effects, we examined whether pitavastatin exerts protective effects on doxorubicin cardiotoxicity. Pretreatment with pitavastatin attenuated doxorubicin-induced oxidative stress, ATM phosphorylation, p53 accumulation, and cardiomyocyte death (Figs. 4(A) and (B)). Statins are known to exert their lipid lowering-independent effects by inhibiting the synthesis of isoprenoids that are critical for posttranslational modification of a variety of proteins [9]. We therefore tested whether pitavastatin attenuates doxorubicin cardiotoxicity through the inhibition of mevalonate-dependent posttranslational protein modifications. Pretreatment with mevalonate, FPP, or GGPP reversed the beneficial effects of pitavastatin on doxorubicin-induced oxidative stress and p53 accumulation (Fig. 4(C)). Likewise, GTI but not FTI reduced doxorubicin-induced oxidative stress and p53 accumulation (Fig. 4(D)), suggesting that the inhibition of protein geranylgeranylation mediates the cardioprotective effects of pitavastatin. Because Rac1 is a major regulator of NADPH oxidase activity and activated by geranylgeranylation but not by farnesylation [14], we next examined the possible involvement of Rac1 in pitavastatin-mediated protective effects against doxorubicin. Indeed, treatment with a Rac1 inhibitor also attenuated doxorubicin-induced oxidative stress and p53 accumulation to the extent comparable with those of pitavastatin and GTI (Fig. 4(D)). Finally, treatment with pitavastatin significantly attenuated chronic doxorubicin treatment-induced cardiomyocyte apoptosis and contractile dysfunction in vivo (Fig. 4(E)), which is consistent with a recent report by others [23]. In cultured myocytes, doxorunbicin augmented NADPH oxidase activity, which was attenuated both by a NADPH oxidase assembly inhibitor (apocynin) and a Rac1 inhibitor (Fig. 4(F)). Furthermore, pitavastatin attenuated Rac1 activity as assessed by subcellular localization (Fig. 4(G)). These results collectively suggest that pitavastatin attenuates doxorubicin cardiotoxicity through its antioxidant effect involving Rac1 inhibition.

4. Discussion

4.1. Doxorubicin induces p53 accumulation in cardiac myocytes through oxidative DNA damage-ATM pathway

Several lines of evidence suggest that oxidative stress and p53 accumulation are involved in doxorubicin-induced cardiotoxicity [1,2]. Consistent with this notion, doxorubicin treatment induced oxidative stress and p53 accumulation both in vitro and in vivo, and reduction of oxidative stress by NAC treatment reduced doxorubicin-induced p53 accumulation in vitro. Because DNA damage is induced by doxorubicin and is a potent inducer of p53 in other cell types [21], we examined whether DNA damage mediates doxorubicin-induced p53 accumulation in cardiac myocytes. Indeed, doxorubicin treatment induced DNA damage and ATM activation, and an ATM kinase inhibitor wortmannin reduced p53 accumulation induced by doxorubicin. These findings are consistent with the notion that ATM activated by DNA damage phosphorylates and stabilizes p53 protein, and suggest that doxorubicin induces p53 accumulation via oxidative DNA damage-ATM pathway. However, it should be noted that p53 accumulation is not completely inhibited by treatment with NAC or wortmannin. It was also reported that the cardioprotective effects of antioxidants are not very remarkable in human clinical trials [24]. Thus, oxidative stress-independent mechanisms may also play a role in doxorubicin-induced p53 accumulation.

4.2. Chronic doxorubicin cardiotoxicity is mediated by p53-dependent cardiomyocyte apoptosis

Previous studies have shown that doxorubicin treatment induces p53 accumulation in the heart, and reduction of p53 activity attenuates deleterious effects of doxorubicin [5,6], suggesting that p53 plays a causal role in doxorubicin cardiotoxicity. Because doxorubicin-induced myocyte apoptosis was reduced by the inhibition of p53 activity, p53-dependent cardiomyocyte apoptosis has been thought to play a crucial role in doxorubicin cardiotoxicity. However, we have recently shown that p53 inhibits the action of hypoxia-inducible factor-1 (Hif-1) and Hif-1-dependent coronary angiogenesis in the heart under chronic pressure overload, leading to contractile dysfunction [7]. More recently, it was shown that p53-induced inhibition of mTOR activity mediates acute doxorubicin cardiotoxicity independently of cardiomyocyte apoptosis [8]. These results suggest that p53-dependent but apoptosis-independent mechanisms may be involved in the pathogenesis of doxorubicin cardiotoxicity. We therefore re-evaluated the role of cardiomyocyte apoptosis in doxorubicin cardiotoxicity using transgenic mice in which cardiomyocyte apoptosis is inhibited by the overexpression of Bcl-2 in the heart, and found that inhibition of myocardial apoptosis significantly improved contractile dysfunction induced by chronic doxorubicin treatment. We also found that doxorubicin treatment did not result in myocardial hypoxia or reduction in myocyte size. Thus, we conclude that chronic doxorubicin cardiotoxicity is mediated by p53-dependent cardiomyocyte apoptosis. These data collectively suggest that, although both acute and chronic doxorubicin cardiotoxicity are mediated by p53, the downstream effectors of p53 in these two situations may be partly distinct. This notion is supported by a transcriptome analysis of acute and chronic doxorubicin cardiotoxicity, in which a different set of genes were up- or down-regulated in the heart after acute and chronic doxorubicin treatment, respectively [25]. It should also be noted that in tumor cell lines, DNA damage induces both p53-dependent and p53-independent apoptosis [26]. Whether DNA damage-dependent p53-independent apoptosis plays a role in doxorubicin cardiotoxicity remains to be elucidated.

4.3. Pitavastatin attenuates doxorubicin cardiotoxicity by inhibiting Rac1 activity

HMG-CoA reductase inhibitors or statins are widely prescribed drugs that inhibit the rate-limiting enzyme for cholesterol synthesis in the liver and lower serum cholesterol levels. However, these drugs also exert cholesterol lowering-independent or pleiotropic effects, many of which are thought to be mediated by their ability to inhibit the synthesis of isoprenoid intermediates required for posttranslational protein modifications. Specifically, isoprenylation of small G proteins such as Ras, Rho or Rac are critical for their proper membrane localization and function, and statin-mediated inhibition of these small G proteins may play a role in the pleiotropic effects of statins. Indeed, our in vitro studies

using isoprenoid intermediates and pharmacological inhibitors strongly suggest that inhibition of Rac1 activation by pitavastatin plays a crucial role in the protective effects of pitavastatin on doxorubicin cardiotoxicity. Because Rac1 is a requisite component of NADPH oxidase, our findings collectively suggest that pitavastatin attenuates doxorubicin cardiotoxicity through its antioxidant effect involving Rac1 inhibition. It was previously shown that oxidative stress is implicated in cardiac hypertrophy and that statins attenuate myocardial hypertrophy through Rac1 inhibition [12], suggesting that similar mechanisms may be involved in the pathogenesis of cardiac hypertrophy and doxorubicin cardiotoxicity.

In summary, we have shown that doxorubicin cardiotoxicity is mediated by oxidative DNA damage-ATM-p53-apoptosis pathway in vitro and in vivo, and attenuated by pitavastatin through its antioxidant effect involving Rac1 inhibition. Further clinical studies are mandatory to determine whether statins are really cardioprotective in the setting of anticancer therapy using doxorubicin or related chemotherapeutic agents.

Acknowledgments

We thank Dr. Michael D. Schneider for Bcl-2 transgenic mice, and E. Fujita, R. Kobayashi, and Y. Ishiyama for technical assistance. This work was supported by grants from the Ministry of Education, Culture, Sports, Science and Technology to IK.

References

[1] Minotti G, Menna P, Salvatorelli E, Cairo G, Gianni L. Anthracyclines: molecular advances and pharmacologic developments in antitumor activity and cardiotoxicity. Pharmacol Rev 2004 Jun;56(2):185–229.
[2] Takemura G, Fujiwara H. Doxorubicin-induced cardiomyopathy from the cardiotoxic mechanisms to management. Prog Cardiovasc Dis 2007 Mar–Apr;49 (5):330–52.
[3] Yen HC, Oberley TD, Vichitbandha S, Ho YS, St Clair DK. The protective role of manganese superoxide dismutase against adriamycin-induced acute cardiac toxicity in transgenic mice. J Clin Invest 1996 Sep 1;98(5):1253–60.
[4] Sun X, Zhou Z, Kang YJ. Attenuation of doxorubicin chronic toxicity in metallothionein-overexpressing transgenic mouse heart. Cancer Res 2001 Apr 15;61(8): 3382–7.
[5] Liu X, Chua CC, Gao J, Chen Z, Landy CL, Hamdy R, et al. Pifithrin-alpha protects against doxorubicin-induced apoptosis and acute cardiotoxicity in mice. Am J Physiol Heart Circ Physiol 2004 Mar;286(3):H933–9.
[6] Shizukuda Y, Matoba S, Mian OY, Nguyen T, Hwang PM. Targeted disruption of p53 attenuates doxorubicin-induced cardiac toxicity in mice. Mol Cell Biochem 2005 May;273(1–2):25–32.
[7] Sano M, Minamino T, Toko H, Miyauchi H, Orimo M, Qin Y, et al. p53-induced inhibition of Hif-1 causes cardiac dysfunction during pressure overload. Nature 2007 Mar 22;446(7134):444–8.
[8] Zhu W, Soonpaa MH, Chen H, Shen W, Payne RM, Liechty EA, et al. Acute doxorubicin cardiotoxicity is associated with p53-induced inhibition of the mammalian target of rapamycin pathway. Circulation 2009 Jan 6;119(1):99–106.
[9] Mital S, Liao JK. Statins and the myocardium. Semin Vasc Med 2004 Nov;4(4): 377–84.
[10] Endres M, Laufs U, Huang Z, Nakamura T, Huang P, Moskowitz MA, et al. Stroke protection by 3-hydroxy-3-methylglutaryl (HMG)-CoA reductase inhibitors mediated by endothelial nitric oxide synthase. Proc Natl Acad Sci U S A 1998 Jul 21;95(15):8880–5.
[11] Lefer AM, Campbell B, Shin YK, Scalia R, Hayward R, Lefer DJ. Simvastatin preserves the ischemic-reperfused myocardium in normocholesterolemic rat hearts. Circulation 1999 Jul 13;100(2):178–84.
[12] Takemoto M, Node K, Nakagami H, Liao Y, Grimm M, Takemoto Y, et al. Statins as antioxidant therapy for preventing cardiac myocyte hypertrophy. J Clin Invest 2001 Nov;108(10):1429–37.
[13] Hasegawa H, Yamamoto R, Takano H, Mizukami M, Asakawa M, Nagai T, et al. 3-Hydroxy-3-methylglutaryl coenzyme A reductase inhibitors prevent the development of cardiac hypertrophy and heart failure in rats. J Mol Cell Cardiol 2003 Aug;35(8):953–60.
[14] Groemping Y, Rittinger K. Activation and assembly of the NADPH oxidase: a structural perspective. Biochem J 2005 Mar 15;386(Pt 3):401–16.
[15] Zou Y, Komuro I, Yamazaki T, Kudoh S, Uozumi H, Kadowaki T, et al. Both Gs and Gi proteins are critically involved in isoproterenol-induced cardiomyocyte hypertrophy. J Biol Chem 1999 Apr 2;274(14):9760–70.
[16] Tanaka M, Nakae S, Terry RD, Mokhtari GK, Gunawan F, Balsam LB, et al. Cardiomyocyte-specific Bcl-2 overexpression attenuates ischemia–reperfusion injury, immune response during acute rejection, and graft coronary artery disease. Blood 2004 Dec 1;104(12):3789–96.
[17] Li SY, Gomelsky M, Duan J, Zhang Z, Gomelsky L, Zhang X, et al. Overexpression of aldehyde dehydrogenase-2 (ALDH2) transgene prevents acetaldehyde-induced cell injury in human umbilical vein endothelial cells: role of ERK and p38 mitogen-activated protein kinase. J Biol Chem 2004 Mar 19;279(12):11244–52.
[18] Szocs K, Lassegue B, Sorescu D, Hilenski LL, Valppu L, Couse TL, et al. Upregulation of Nox-based NAD(P)H oxidases in restenosis after carotid injury. Arterioscler Thromb Vasc Biol 2002 Jan;22(1):21–7.
[19] Deng S, Kruger A, Kleschyov AL, Kalinowski L, Daiber A, Wojnowski L. Gp91phox-containing NAD(P)H oxidase increases superoxide formation by doxorubicin and NADPH. Free Radic Biol Med 2007 Feb 15;42(4):466–73.
[20] Spallarossa P, Garibaldi S, Altieri P, Fabbi P, Manca V, Nasti S, et al. Carvedilol prevents doxorubicin-induced free radical release and apoptosis in cardiomyocytes in vitro. J Mol Cell Cardiol 2004 Oct;37(4):837–46.
[21] L'Ecuyer T, Sanjeev S, Thomas R, Novak R, Das L, Campbell W, et al. DNA damage is an early event in doxorubicin-induced cardiac myocyte death. Am J Physiol Heart Circ Physiol 2006 Sep;291(3):H1273–80.
[22] Kurz EU, Douglas P, Lees-Miller SP. Doxorubicin activates ATM-dependent phosphorylation of multiple downstream targets in part through the generation of reactive oxygen species. J Biol Chem 2004 Dec 17;279(51):53272–81.
[23] Riad A, Bien S, Westermann D, Becher PM, Loya K, Landmesser U, et al. Pretreatment with statin attenuates the cardiotoxicity of Doxorubicin in mice. Cancer Res 2009 Jan 15;69(2):695–9.
[24] Ladas EJ, Jacobson JS, Kennedy DD, Teel K, Fleischauer A, Kelly KM. Antioxidants and cancer therapy: a systematic review. J Clin Oncol 2004 Feb 1;22(3):517–28.
[25] Yi X, Bekeredjian R, DeFilippis NJ, Siddiquee Z, Fernandez E, Shohet RV. Transcriptional analysis of doxorubicin-induced cardiotoxicity. Am J Physiol Heart Circ Physiol 2006 Mar;290(3):H1098–102.
[26] Roos WP, Kaina B. DNA damage-induced cell death by apoptosis. Trends Mol Med 2006 Sep;12(9):440–50.

Cardiac mast cells cause atrial fibrillation through PDGF-A–mediated fibrosis in pressure-overloaded mouse hearts

Chien-hui Liao,[1,2] Hiroshi Akazawa,[1] Masaji Tamagawa,[3] Kaoru Ito,[1] Noritaka Yasuda,[1] Yoko Kudo,[1] Rie Yamamoto,[1] Yukako Ozasa,[1] Masanori Fujimoto,[1] Ping Wang,[1] Hiromitsu Nakauchi,[2] Haruaki Nakaya,[3] and Issei Komuro[1]

[1]Department of Cardiovascular Science and Medicine, Chiba University Graduate School of Medicine, Chiba, Japan. [2]Division of Stem Cell Therapy, Center for Stem Cell and Regenerative Medicine, Institute of Medical Science, University of Tokyo, Tokyo, Japan. [3]Department of Pharmacology, Chiba University Graduate School of Medicine, Chiba, Japan.

Atrial fibrillation (AF) is a common arrhythmia that increases the risk of stroke and heart failure. Here, we have shown that mast cells, key mediators of allergic and immune responses, are critically involved in AF pathogenesis in stressed mouse hearts. Pressure overload induced mast cell infiltration and fibrosis in the atrium and enhanced AF susceptibility following atrial burst stimulation. Both atrial fibrosis and AF inducibility were attenuated by stabilization of mast cells with cromolyn and by BM reconstitution from mast cell–deficient WBB6F1-*Kit*$^{W/W\text{-}v}$ mice. When cocultured with cardiac myocytes or fibroblasts, BM-derived mouse mast cells increased platelet-derived growth factor A (PDGF-A) synthesis and promoted cell proliferation and collagen expression in cardiac fibroblasts. These changes were abolished by treatment with a neutralizing antibody specific for PDGF α-receptor (PDGFR-α). Consistent with these data, upregulation of atrial *Pdgfa* expression in pressure-overloaded hearts was suppressed by BM reconstitution from WBB6F1-*Kit*$^{W/W\text{-}v}$ mice. Furthermore, injection of the neutralizing PDGFR-α–specific antibody attenuated atrial fibrosis and AF inducibility in pressure-overloaded hearts, whereas administration of homodimer of PDGF-A (PDGF-AA) promoted atrial fibrosis and enhanced AF susceptibility in normal hearts. Our results suggest a crucial role for mast cells in AF and highlight a potential application of controlling the mast cell/PDGF-A axis to achieve upstream prevention of AF in stressed hearts.

Introduction

Atrial fibrillation (AF) is a supraventricular arrhythmia that is characterized by rapid and fibrillatory atrial activation with an irregular ventricular response. AF remains the most common arrhythmia encountered in clinical practice and is associated with an increased risk of stroke, heart failure, and overall mortality (1). Several cardiovascular disorders predispose to AF, such as coronary artery disease, valvular heart disease, congestive heart failure, and hypertension, especially when LV hypertrophy is present (1). Recent electrophysiological evidence has indicated that the triggering ectopic foci act on predisposing substrates to initiate single- or multiple-circuit reentry, leading to AF (2). The most important histopathological change in AF is atrial fibrosis (3, 4). Accumulation of ECM proteins has been documented in biopsied specimens of atrium from patients with AF (5), and experimental studies using animal models have indicated that interstitial deposition of dense ECM proteins causes separation between bundles of atrial myocytes and disturbs cell-to-cell impulse propagation (3, 4). In addition, atrial fibrosis potentially exaggerates myocardial ischemia by hampering oxygen diffusion and alters the electrophysical and biomechanical properties of atrial myocytes, allowing the initiation and perpetuation of AF (4). The mechanisms underlying the development of atrial fibrosis in AF remain unclear, but evolving evidence has suggested that inflammation is profoundly implicated in the process of the structural remodeling in the atrium (4, 6). Inflammatory infiltrates were observed in the atrium of AF patients and animal models (7, 8). Furthermore, inflammatory biomarkers such as C-reactive protein were elevated in AF patients and were associated with the presence of AF and the future development of AF (9, 10). However, it remains to be fully elucidated how inflammation is linked to the development of structural remodeling as a susceptible AF substrate in stressed hearts.

Mast cells function as key effector cells during allergic and immune responses through releasing preformed or newly synthesized bioactive products (11). Recent studies have implicated mast cells in inflammation and tissue remodeling (11, 12). Indeed, mast cells reside in many tissues including the heart (13) and participate in the inflammatory process underlying several cardiovascular disorders, such as atherosclerosis (14, 15), aortic aneurysm (16, 17), heart failure (18), viral myocarditis (19), and ventricular arrhythmia during ischemia/reperfusion injury (20). In particular, mast cell–derived IL-6 and IFN-γ have been reported to promote atherosclerosis and abdominal aortic aneurysm (15, 16). Meanwhile, mast cells enhance the fibrogenic process through the release of multiple proteases and inflammatory cytokines in the skin, lung, and kidney (21–24). Here, we demonstrate that mast cells infiltrate the atrium of pressure-overloaded mice and contribute to the pathogenesis of atrial fibrosis and AF susceptibility. Mechanistically, upregulation of PDGF-A mediates the fibrogenic effect of mast cells in promoting AF. These results provide mechanistic insights into the pathogenic role of mast cells in promoting an AF substrate in stressed hearts.

Conflict of interest: The authors have declared that no conflict of interest exists.
Citation for this article: *J. Clin. Invest.* **120**:242–253 (2010). doi:10.1172/JCI39942.

Table 1
Echocardiographic measurements in TAC- and sham-operated mice with or without treatment with cromolyn

	Sham		TAC	
Cromolyn	(–)	(+)	(–)	(+)
Number	10	5	17	15
HW/BW (mg/g)	4.55 ± 0.11	4.64 ± 0.04	5.24 ± 0.05[A]	5.54 ± 0.13[A]
HR (bpm)	610.10 ± 7.59	613.20 ± 3.44	599.24 ± 7.30	622.67 ± 7.05
LVDd (mm)	3.58 ± 0.08	3.51 ± 0.08	3.55 ± 0.04	3.54 ± 0.09
LVDs (mm)	1.99 ± 0.06	2.06 ± 0.05	2.05 ± 0.04	1.97 ± 0.07
FS (%)	44.5 ± 0.87	41.2 ± 0.99	42.2 ± 0.62	44.6 ± 0.91
LVPWth (mm)	0.65 ± 0.11	0.64 ± 0.04	0.81 ± 0.01[A]	0.82 ± 0.01[A]

[A]$P < 0.01$ versus sham. FS, fractional shortening; HR, heart rate; HW/BW, heart-to-body weight ratio; LVDd, LV diameter in end diastole; LVDs, LV diameter in end systole; LVPWth, LV posterior wall thickness in end diastole.

Results

Atrial burst stimulation induces AF in pressure-overloaded hearts. To develop a model of AF associated with LV hypertrophy, we first induced pressure overload in mice by producing transverse aorta constriction (TAC) (25). On day 10, TAC-operated mice showed a significant increase in heart-to-body weight and LV wall thickness with preserved fractional shortening (Table 1). The atrium-to-body weight ratios were increased 36%, from 0.22 ± 0.02 mg/g in sham-operated mice ($n = 5$) to 0.30 ± 0.02 mg/g in TAC-operated mice ($n = 5$; $P < 0.01$), indicating that TAC operation induced hemodynamic overload in both the atrium and ventricle. We recorded ECGs using telemetry at 10 days after the operation, but no episode of spontaneous AF was observed in TAC- or sham-operated mice (Supplemental Figure 1; supplemental material available online with this article; doi:10.1172/JCI39942DS1).

To test the inducibility of AF, we applied programmed electrical stimulation directly to right atrium under Langendorff perfusion at 10 days after the operation. During the period for stabilization prior to stimulation, spontaneous episodes of AF were not observed in TAC- or sham-operated hearts. However, the induction of AF was attainable and reliably reproducible with programmed electrical stimulation of right atrium (Figure 1A). AF was defined as an episode of rapid and chaotic atrial rhythm and irregular ventricular response. AF was induced more frequently in TAC-operated hearts (100%) than in sham-operated hearts (20%) (Figure 1, A–C). In addition, the duration of AF episodes in TAC-operated hearts was significantly longer than that in sham-operated hearts (Figure 1D). We also applied atrial stimulation under Langendorff perfusion at 28 days after TAC operation. However, TAC-operated hearts showed severe LV dysfunction (fractional shortening, 16.6% ± 8.4%) at this time point, and undesirable arrhythmias such as ventricular fibrillation were induced each time after stimulation, which hampered our evaluation of AF arrhythmogenesis. Therefore, atrial burst stimulation under Langendorff perfusion at 10 days after TAC operation represents a valid ex vivo model that permits study of AF substrate, especially in the setting of LV hypertrophy.

Mast cells are accumulated and activated in the atrium of TAC-operated mice. To assess the contribution of mast cells to atrial arrhythmogenicity, we evaluated the contents of mast cells in atrium by staining histological sections with toluidine blue. The number of infiltrating mast cells showed a 2.5-fold increase in TAC-operated mice on day 10, as compared with sham-operated mice (Figure 2A). Avidin conjugated to fluorochrome dyes binds to the negatively charged heparin proteoglycans and identifies the granules of mast cells (20, 26). In the left and right atria of TAC-operated mice, we observed a marked increase of mast cell activation with the presence of extruded avidin-positive granules close to cell surface (Figure 2B). These results suggest that mast cells are accumulated and activated in the atrium of pressure-overloaded hearts.

Stabilization of mast cells by cromolyn attenuates AF in TAC-operated hearts. Accumulation of mast cells in the atrium indicated a causal link between infiltration of these cells and the pathogenesis of AF. To determine the importance of mast cells in this process, we systemically administered the mast cell stabilizer cromolyn (14, 20) to TAC-operated mice. In the atrium at 10 days after TAC operation, the degranulation of mast cells was almost completely inhibited by cromolyn treatment (Figure 2B), although the mast cell contents were not significantly decreased ($P = 0.17$; Figure 2A). Echocardiographic parameters regarding LV hypertrophy and systolic function remained unchanged by cromolyn treatment (Table 1). As revealed by histology, there was no significant difference in the average size of ventricular myocytes between cromolyn- and vehicle-treated mice (Supplemental Figure 2). In addition, the atrium-to-body weight ratios at 10 days after TAC operation were not significantly different between cromolyn- and vehicle-treated mice (0.30 ± 0.02 mg/g vs. 0.28 ± 0.02 mg/g; $P = 0.43$). These results suggest that cromolyn did not affect the hemodynamic workload. However, as compared with vehicle-treated mice, cromolyn-treated mice showed a remarkable reduction in the incidence and duration of AF episodes after atrial burst stimulation under Langendorff perfusion (Figure 3, A–C). To validate and extend our ex vivo findings, we subjected anesthetized mice to rapid transesophageal atrial pacing and simultaneous surface ECG recording at 10 days after the operation. AF could be induced in vivo after atrial burst stimulation in TAC-operated mice, but not in sham-operated mice (Figure 3, D–F). Similarly, cromolyn treatment completely suppressed AF induced by transesophageal atrial pacing in TAC-operated mice (Figure 3, G and H).

Atrial fibrosis is a major feature of structural remodeling that contributes to AF substrate (3, 4). In the atrium of TAC-operated mice, Masson's trichrome staining revealed areas of interstitial fibrosis (Figure 3I), and hydroxyproline assay indicated deposition of collagen (Figure 3J). Mast cell stabilization by cromolyn remarkably attenuated fibrotic changes in the atrium of TAC-operated mice (Figure 3, I and J). These results suggest that stabilization of mast cells prevents atrial structural remodeling and AF inducibility in TAC-operated mice.

Reconstitution with BM cells from mast cell–deficient W/W^v mice attenuates AF in TAC-operated hearts. To further examine the role of mast cells in AF, we utilized mast cell–deficient *WBB6F1-Kit$^{W/W\text{-}v}$* (W/W^v) mice carrying compound heterozygous mutations of *c-kit* (*Kit^W*, null; *Kit$^{W\text{-}v}$*, dominant negative). To circumvent the undesirable effects by altered c-kit signaling in nonhematopoietic cells, we reconstituted C57BL/6 mice with BM cells from W/W^v mice or control *WBB6F1-Kit$^{+/+}$* (+/+) mice. We first confirmed, by tolu-

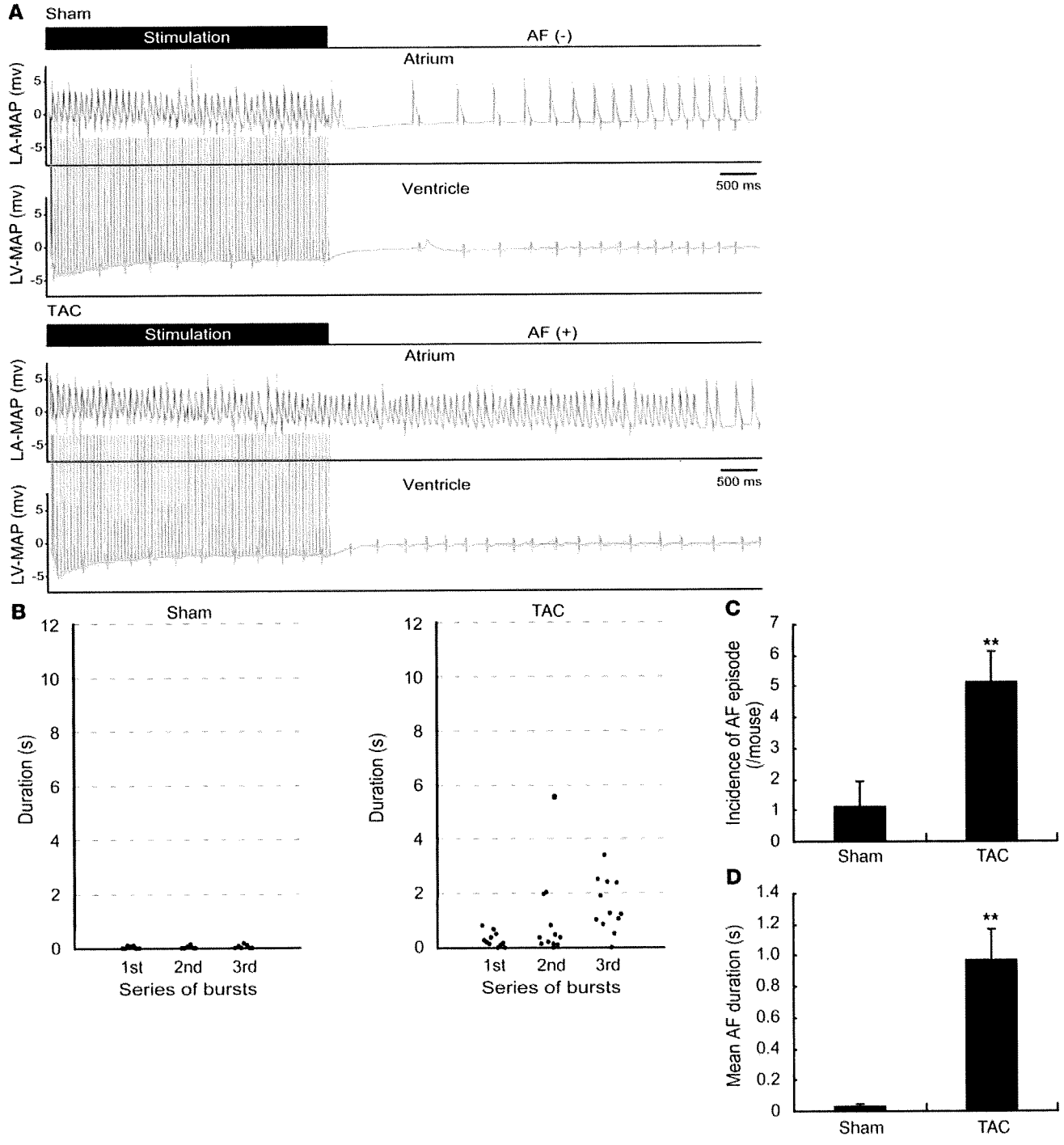

Figure 1
Induction of AF in Langendorff-perfused hearts of mice after TAC operation. (**A**) Termination of the burst of atrial stimulation triggers AF, characterized by rapid and chaotic atrial rhythm and irregular ventricular response, in Langendorff-perfused hearts undergoing TAC operation (lower panels), but not sham operation (upper panels). LA-MAP, monophasic action potential of left atrium; LV-MAP, monophasic action potential of LV. (**B**) AF was triggered in mice undergoing TAC ($n = 5$) or sham ($n = 5$) operation by applying 3 series of bursts with 5-minute intervals. The duration of AF episode occurring after each burst is plotted. (**C**) Incidence of AF episodes during 3 series of bursts in mice undergoing TAC ($n = 5$) or sham ($n = 5$) operation. (**D**) Mean duration of AF episodes during 3 series of bursts in mice undergoing TAC ($n = 5$) or sham ($n = 5$) operation. $^{**}P < 0.01$ versus sham. Data are presented as mean ± SEM.

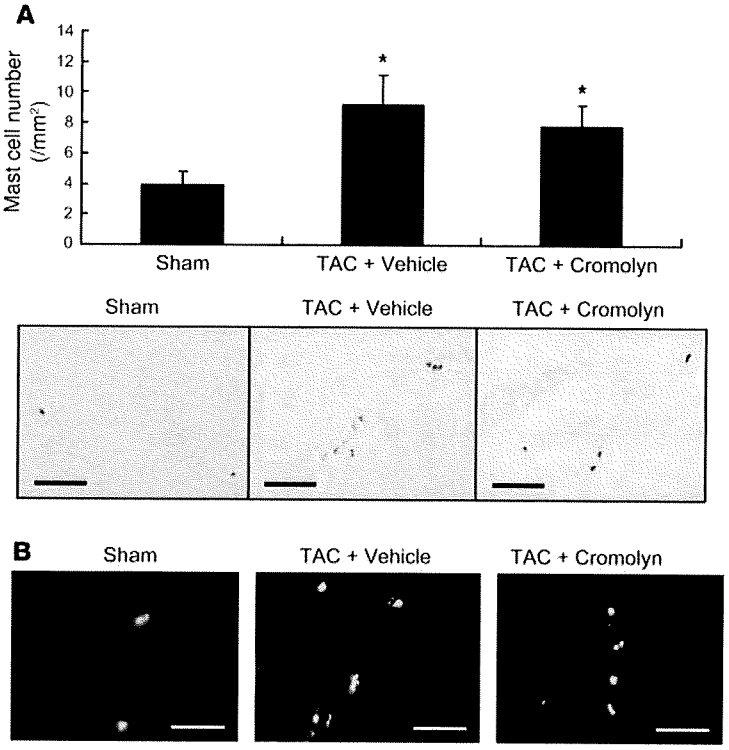

Figure 2

Stabilization of mast cells infiltrating the atrium of TAC-operated mice by cromolyn. (**A**) Representative histological sections with toluidine blue staining for detection of mast cells (purple) in the atrium. Wild-type mice were treated with cromolyn (n = 7) or vehicle (n = 8), and subjected to TAC operation. Mast cell content on day 10 was presented as mean ± SEM. Sham-operated mice were used as control (n = 5). *P < 0.05 versus sham. (**B**) Rhodamine-avidin staining for visualization of mast cell degranulation. Scale bars: 10 μm (**A**); 5 μm (**B**).

idine blue staining, that mast cells were not present in the atrium of mice reconstituted with BM cells from W/W^v mice (W/W^v-BMT mice) after TAC operation, although abundant mast cells infiltrated the atrium of mice reconstituted with BM cells from +/+ mice (+/+-BMT mice) after TAC operation (Figure 4A). Echocardiographic examination revealed that LV hypertrophy after TAC operation did not significantly differ between W/W^v-BMT and +/+-BMT mice, but the fractional shortening in W/W^v-BMT mice was slightly decreased compared with that in +/+-BMT mice (Table 2). In spite of the reduced LV systolic function after TAC operation, the atrium-to-body weight ratios were not significantly different between +/+-BMT mice and W/W^v-BMT mice (0.27 ± 0.02 mg/g vs. 0.31 ± 0.05 mg/g; P = 0.54), and reconstitution with W/W^v BM induced a marked reduction in the incidence and duration of AF episode after atrial burst stimulation compared with +/+ BM reconstitution (Figure 4, B–D). In addition, histological analysis and hydroxyproline assay revealed that atrial fibrosis after TAC operation was attenuated in W/W^v-BMT mice compared with +/+-BMT mice (Figure 4, E and F). These results suggest that deficiency of mast cells prevents atrial structural remodeling and AF inducibility in TAC-operated mice.

BM-derived mast cells cocultured with cardiac myocytes or fibroblasts release PDGF-A to promote fibrinogenesis. In response to a variety of stimuli, mast cells are activated and release numerous bioactive effectors that, either prestored or de novo synthesized, mediate immunoregulatory and proinflammatory effects (11, 24). To delineate mast cell–derived effectors that are involved in the promotion of atrial fibrosis, we examined the gene expressions of fibrosis-related effectors in BM-derived mast cells (BMMCs) after coculture with cardiac myocytes or fibroblasts (Figure 5, A and B, and Supplemental Figure 3). Notably, in quantitative real-time RT-PCR analysis, the mRNA levels of murine *Pdgfa* in BMMCs were prominently elevated after 6 hours coculture with neonatal rat cardiac myocytes or fibroblasts (Figure 5, A and B, and Supplemental Figure 3). In addition, the expression levels of *Pdgfa* were upregulated in the atrium at 10 days after TAC operation, and they were significantly attenuated by reconstitution with W/W^v BM (Figure 5C). These results suggest that mast cells infiltrating the atrium are activated to increase *Pdgfa* gene expression.

Next, we assayed the concentrations of PDGF-AA in medium conditioned by coculture of BMMCs and cardiac fibroblasts. The PDGF-AA concentration showed a more than 3-fold increase after 6 hours coculture, and this increase was remarkably blunted by stabilization of BMMCs with cromolyn during the coculture (Figure 6A). The conditioned medium of coculture promoted cell proliferation of cardiac fibroblasts, and the proliferative effects were abrogated by addition of a neutralizing anti-PDGF α-receptor (anti–PDGFR-α) antibody to the conditioned medium (Figure 6B). Furthermore, the expression of *Col3a1* in cardiac fibroblasts was upregulated after coculture with BMMC, and it was blunted by the treatment with cromolyn or anti–PDGFR-α antibody (Figure 6C). Thus, BMMC-derived PDGF-A can induce cell proliferation and collagen gene expression in cardiac fibroblasts. These results raise a possibility that infiltrating mast cells promote atrial fibrosis and AF inducibility in a PDGF-A–mediated pathway.

Administration of PDGF-AA enhances AF susceptibility in normal hearts. To examine functional significance of atrial *Pdgfa* upregulation in the development of AF substrate, we administered PDGF-AA or vehicle to nonoperated mice and applied atrial burst stimulation. Administration of PDGF-AA for 10 days induced systemic tissue fibrosis, which was particularly prominent in atrium as compared with ventricle (Figure 7A). As a consequence, PDGF-AA–treated hearts showed a significant increase in the incidence and duration of AF episode after atrial burst stimulation under Langendorff perfusion compared with vehicle-treated hearts (Figure 7, B–D). These results suggest that upregulation of *Pdgfa* in atrium can induce atrial fibrosis and enhance AF inducibility in normal hearts.

Neutralization of PDGFR-α attenuates AF in TAC-operated hearts. Next, to examine the role of PDGF-A in the pathogenesis of AF substrate, we inhibited the actions of PDGF-A in TAC-operated hearts by systemic injection of a neutralizing antibody against PDGFR-α (APA5) (27). At 10 days after TAC operation, LV hypertrophy and contraction, as assessed by echocardiography, did not significantly differ between neutralizing antibody–treated mice (TAC-APA5 mice) and control IgG2a-treated mice (TAC-IgG mice) (Table 3). In addition, the atrium-to-body weight ratios were not significantly different between TAC-APA5 and TAC-IgG mice (0.34 ± 0.02 mg/g vs. 0.31 ± 0.03 mg/g; P = 0.44). However, neutralization of PDGFR-α induced a marked reduction

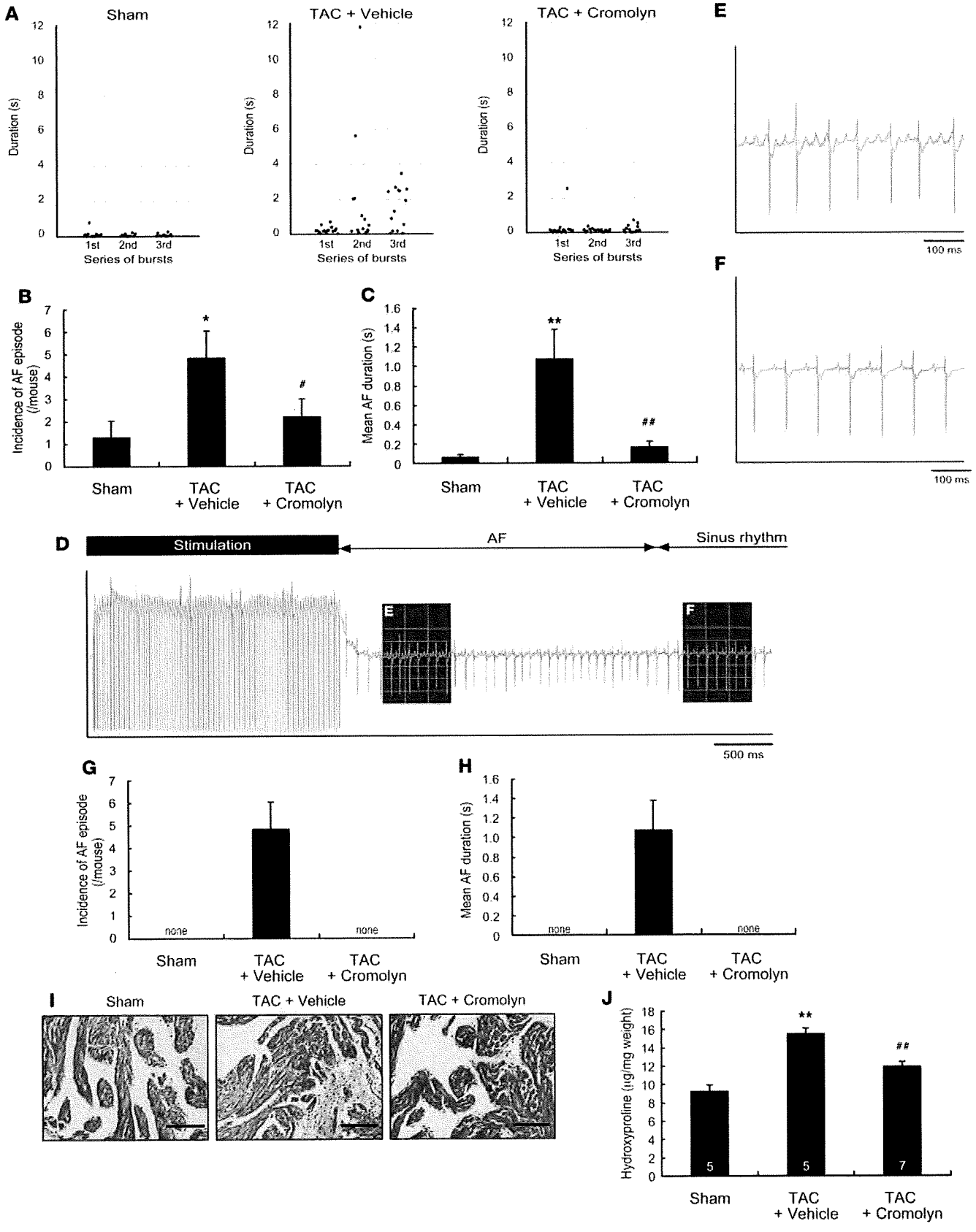
A
Sham
TAC + Vehicle
TAC + Cromolyn
Duration (s)
Series of bursts
1st
2nd
3rd
E
100 ms
F
100 ms
B
Incidence of AF episode (/mouse)
Sham
TAC + Vehicle
TAC + Cromolyn
C
Mean AF duration (s)
D
Stimulation
AF
Sinus rhythm
500 ms
G
H
none
I
J
Hydroxyproline (μg/mg weight)

Figure 3
Attenuation of AF and atrial fibrosis by mast cell stabilization by cromolyn. (**A**) Scatter plot of the duration of AF episodes occurring during 3 series of bursts in Langendorff-perfused hearts (n = 10). (**B**) Incidence of AF episodes during 3 series of bursts under Langendorff perfusion (n = 10). *P < 0.05 versus sham; #P < 0.05 versus TAC treated with vehicle. (**C**) Mean duration of AF episodes during 3 series of bursts under Langendorff perfusion (n = 10). **P < 0.01 versus sham; ##P < 0.01 versus TAC treated with vehicle. (**D**) Representative surface ECG in lead-II deflection of AF induced by termination of the burst of transesophageal atrial pacing in TAC-operated mice. (**E**) High-magnification view of the section delineated by shaded box in **D**, showing AF with chaotic atrial rhythm and irregular ventricular response. (**F**) High-magnification view of the section delineated by shaded box in **D**. AF was spontaneously converted to sinus rhythm. (**G**) Incidence of AF episodes during 3 series of transesophageal bursts (n = 6). (**H**) Mean duration of AF episodes during 3 series of transesophageal bursts (n = 6). (**I**) Representative histological sections with Masson's trichrome staining for visualization of atrial fibrosis (blue staining). Scale bars: 20 μm. (**J**) Hydroxyproline content in the atrium. Number of mice for each experiment is indicated in the bars. **P < 0.01 versus sham; ##P < 0.01 versus TAC treated with vehicle. Data are presented as mean ± SEM.

in the incidence and duration of AF episode both after atrial burst stimulation under Langendorff perfusion (Figure 8, A–C) and after transesophageal atrial pacing in vivo (Figure 8, D and E). In addition, histological analysis and hydroxyproline assay revealed that atrial fibrosis was attenuated in TAC-APA5 mice compared with TAC-IgG mice (Figure 8, F and G). Thus, the effects of cromolyn treatment or BM reconstitution from W/W^v mice on AF substrate were reproduced by neutralization of PDGFR-α in TAC-operated hearts. These results suggest that PDGF-A mediates the deleterious effects of mast cells to promote atrial fibrosis and AF inducibility.

Discussion

Clinical and experimental studies have suggested that inflammation underlies a susceptible AF substrate, which is characterized by interstitial fibrosis in atrium. Our present study demonstrated a hitherto unknown role of mast cells in the development of a susceptible AF substrate. Mast cells were accumulated and activated in the atrium of pressure-overloaded mice, and pharmacological stabilization or genetic depletion of mast cells prevented atrial structural remodeling and reduced the incidence and duration of AF following atrial burst stimulation. Notably, infiltrating mast cells induced upregulation of PDGF-A in the atrium, and neutral-

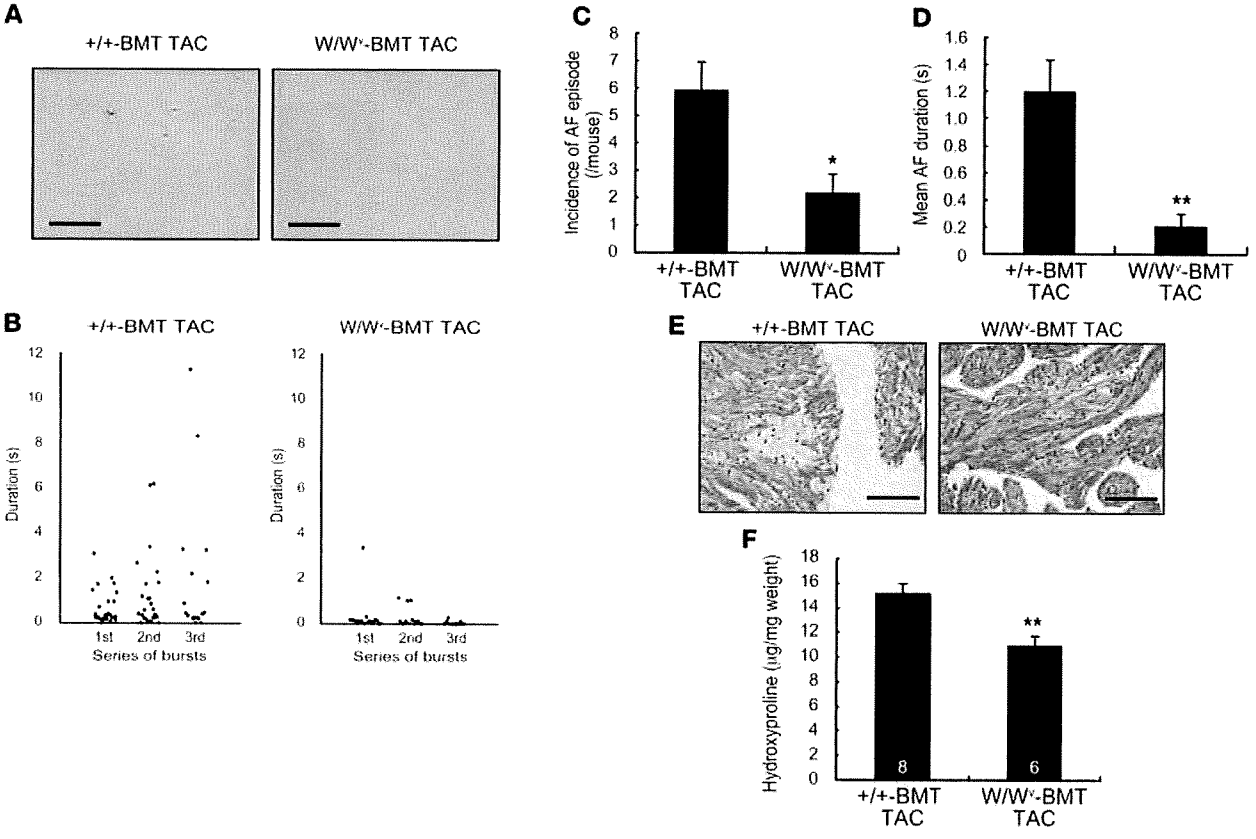

Figure 4
Attenuation of atrial fibrosis and AF by reconstitution with BM cells from W/W^v mice. (**A**) Representative histological sections with toluidine blue staining. Mast cells were not present in the atrium of TAC-operated W/W^v-BMT mice. (**B**) Scatter plot of the duration of AF episodes occurring during 3 series of bursts in TAC-operated W/W^v-BMT mice (n = 11) or +/+-BMT mice (n = 11). (**C**) Incidence of AF episodes during 3 series of bursts (n = 11). *P < 0.05 versus +/+-BMT mice. (**D**) Mean duration of AF episodes during 3 series of bursts (n = 11). **P < 0.01 versus +/+-BMT mice. (**E**) Representative histological sections with Masson's trichrome staining for visualization of atrial fibrosis (blue staining). (**F**) Hydroxyproline content in the atrium. Number of mice for each experiment is indicated in the bars. Scale bars: 10 μm (**A**); 20 μm (**E**). Data are presented as mean ± SEM.

Table 2
Echocardiographic measurements in TAC- or sham-operated W/W^v-BMT or +/+-BMT mice

	Sham		TAC	
	+/+-BMT	W/W^v-BMT	+/+-BMT	W/W^v-BMT
Number	9	9	9	9
HW/BW (mg/g)	4.42 ± 0.14	4.42 ± 0.13	5.51 ± 0.10^A	5.34 ± 0.16^A
HR (bpm)	636.63 ± 7.78	629.22 ± 2.89	613.20 ± 9.34	612.33 ± 6.78
LVDd (mm)	3.68 ± 0.05	3.61 ± 0.07	3.55 ± 0.07	3.69 ± 0.07
LVDs (mm)	2.30 ± 0.05	2.15 ± 0.05	2.05 ± 0.04^A	2.28 ± 0.08^B
FS (%)	39.3 ± 0.93	40.4 ± 0.44	41.6 ± 0.26^C	38.96 ± 1.32^D
LVPWth (mm)	0.61 ± 0.01	0.58 ± 0.01	0.68 ± 0.01^A	0.66 ± 0.02^A

$^AP < 0.01$ versus sham. $^BP < 0.01$ versus TAC-operated +/+-BMT. $^CP < 0.05$ versus sham. $^DP < 0.05$ versus TAC-operated ++-BMT.

ization of PDGFR-α prevented atrial fibrosis and AF inducibility, indicating a pivotal role of PDGF-A in mast cell–triggered AF. It has been reported that atrial arrhythmias and fibrillation occur with extremely low frequency in mice because the atrium is too small in size to maintain multiple-circuit reentry (28). Indeed, we did not detect any spontaneous episode of AF in TAC-operated mice by ECG telemetry (Supplemental Figure 1), but atrial burst stimulation reproducibly induced AF either in ex vivo or in vivo hearts subjected to pressure overload (Figures 1 and 3). Although the duration of AF was limited in length as compared with that in large animal models, a mouse model is powerful for dissection of the causal relationship between arrhythmogenesis and genetic or cellular factors. Although transesophageal pacing in vivo is minimally invasive for atrial stimulation, the incidence of AF was relatively low even in TAC-operated mice (50%), and an anesthetic agent might influence the inducibility and duration of AF in an in vivo model (28). In this regard, atrial stimulation under Langendorff perfusion is a suitable and reliable model of AF that provides mechanistic and therapeutic insights into development of an AF substrate in the setting of hemodynamic overload.

Besides orchestrating allergic and immune responses, mast cells participate in the inflammatory process that underlies the development of cardiovascular diseases (11). Insomuch as the number of infiltrating mast cells at the affected lesions is significantly increased but yet relatively low, it has been difficult to characterize the relevance of these cells to the pathogenesis of a disease. However, mice genetically deficient for mast cells allow assessment of

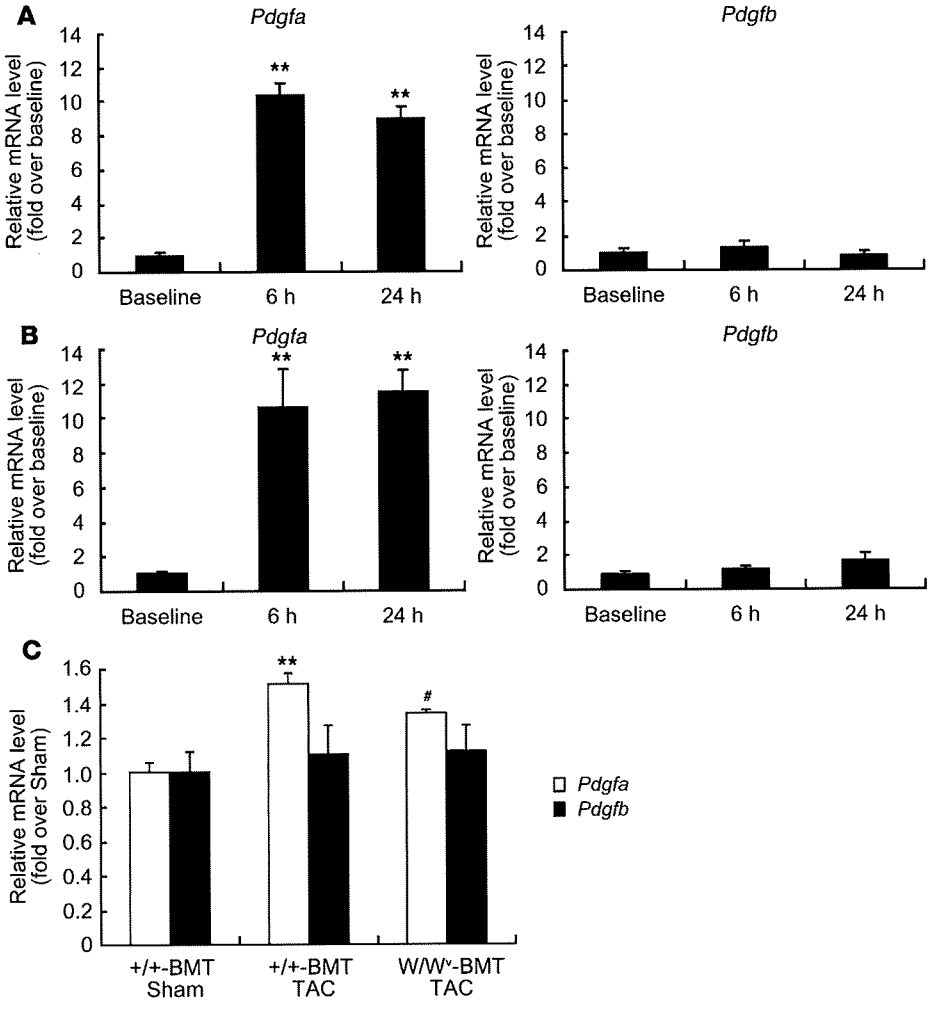

Figure 5
Mast cell–mediated upregulation of *Pdgfa* expression in the atrium of TAC-operated hearts. (**A**) mRNA expression of *Pdgfa* and *Pdgfb* in BMMCs at baseline, 6 hours, and 24 hours after coculture with cardiac myocytes. Experiments were repeated 4 times in triplicate. $^{**}P < 0.01$ versus baseline. (**B**) mRNA expressions of *Pdgfa* and *Pdgfb* in BMMCs at baseline, 6 hours, and 24 hours after coculture with cardiac fibroblasts. Experiments were repeated 5 times in triplicate. $^{**}P < 0.01$ versus baseline. (**C**) mRNA expressions of *Pdgfa* and *Pdgfb* in the atrium of sham-operated mice ($n = 8$), TAC-operated W/W^v-BMT mice (W/W^v-BMT TAC, $n = 7$), or +/+ mice (+/+-BMT TAC, $n = 6$). $^{**}P < 0.01$ versus sham; $^{\#}P < 0.05$ versus +/+-BMT TAC. Data are presented as mean ± SEM.

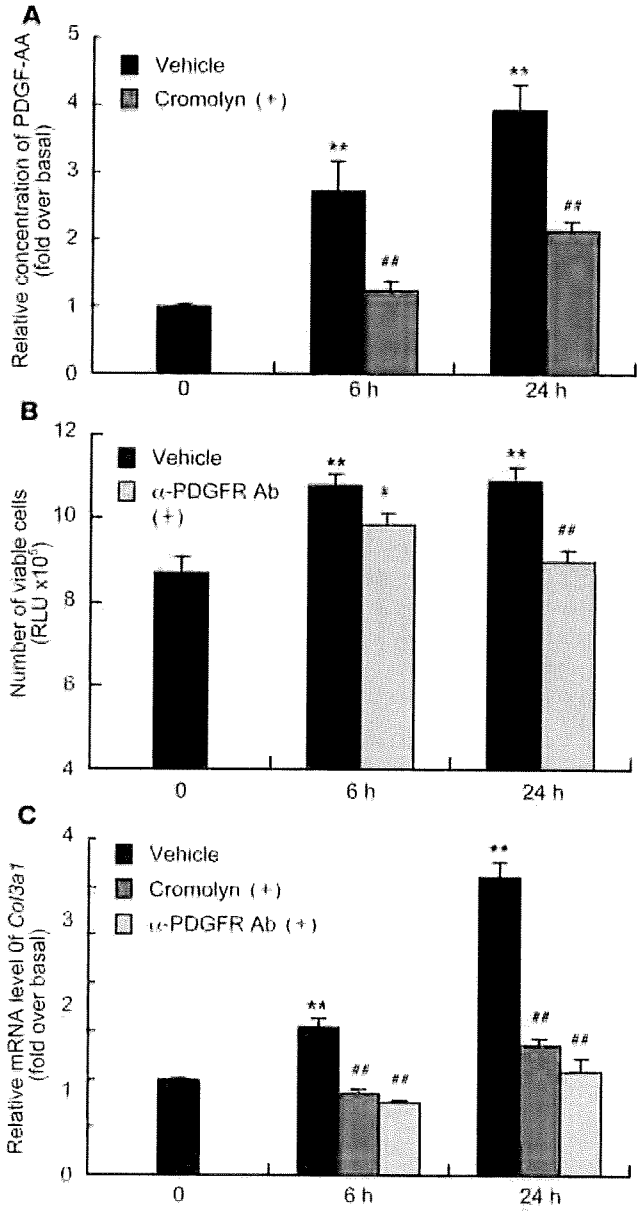

Figure 6

BMMC-derived PDGF-A can induce cell proliferation and collagen gene expression in cardiac fibroblasts. (**A**) ELISA analysis of PDGF-AA content in conditioned medium at baseline, 6 hours, and 24 hours after coculture of BMMCs and cardiac fibroblasts with or without cromolyn (10 μM). Experiments were repeated 5 times in triplicate. $^{**}P < 0.01$ versus baseline; $^{\#\#}P < 0.01$ versus vehicle. (**B**) Number of viable cardiac fibroblasts at baseline, 6 hours, and 24 hours after culture in medium-conditioned coculture of BMMCs and cardiac fibroblasts with or without a neutralizing anti–PDGFR-α antibody (2 μg/ml), as assessed by relative amount of ATP. Experiments were repeated 4 times in triplicate. $^{**}P < 0.01$ versus baseline; $^{\#}P < 0.05$; $^{\#\#}P < 0.01$ versus vehicle. (**C**) mRNA expressions of *Col3a1* in cardiac fibroblasts cocultured with BMMCs with or without cromolyn (10 μM) or a neutralizing anti–PDGFR-α antibody (2 μg/ml) at baseline, 6 hours, and 24 hours. Experiments were repeated 4 times in triplicate. $^{**}P < 0.01$ versus baseline; $^{\#\#}P < 0.01$ versus vehicle. Data are presented as mean ± SEM.

the contributions of mast cell function to biological responses in vivo (11). In this study, we utilized *c-kit* mutant W/W^v mice that are profoundly mast cell deficient (29) and virtually lack melanocytes and interstitial Cajal cells (30). According to a recent paper, *c-kit* is also expressed in cardiac stem cells and cardiac myocytes and plays a regulatory role in the differentiation of these cells (31). Thus, to avoid the effects of *c-kit* mutation on cardiac myocytes, we reconstituted C57BL/6 mice with BM from W/W^v mice. BM reconstitution from W/W^v mice influenced contractile function, which might be related to hematological abnormalities such as macrocytic anemia (32). In spite of the hemodynamic burden, atrial structural remodeling and AF susceptibility were blunted by BM reconstitution from W/W^v mice, which underpinned the functional importance of mast cells in the AF pathogenesis of pressure-overloaded hearts.

Mast cells exist in the heart under physiological conditions (13), and mast cell density in heart tissues of patients with cardiomyopathy is elevated, as compared with normal hearts (33). Mast cells are long lived in the tissue and can reenter cell cycle and proliferate locally (34). A variety of chemokines have been identified that induce local recruitment of mast cells, such as SCF, monocyte chemoattraction protein-1 (MCP-1), nerve growth factor (NGF), and RANTES (24). In addition, interactions between mast cells and connective tissue matrix components have profound influences on the distribution of mast cells in tissues (35–37). Although the most important trigger for mast cell activation is antigen- and IgE-dependent aggregation of IgE receptor (FcεRI), mast cells can be activated by various factors, such as cytokines, growth factors, and hormones (11, 12, 24). In our study, coculture with cardiac myocytes or fibroblasts per se promoted gene expression of some cytokines in BMMCs. We postulate that a certain paracrine- or cell-to-cell contact–dependent signaling may trigger mast cell activation in hearts. Further investigation will be required to delineate the precise mechanisms of how cardiac mast cells are accumulated and activated in stressed hearts.

Mast cells secrete diverse chemical mediators, cytokines, and growth factors upon exposure to a stimulus. This process involves release of the mediators prestored in the granules (degranulation) and de novo synthesis of mediators. Differential synthesis of mast cell mediators is dependent on the particular mechanism of activation and the strength of the stimulus and is crucially involved in the inflammatory process (12, 24). We identified PDGF-A as a crucial molecule that mediates mast cell–induced atrial fibrosis. Among the fibrogenic mediators, upregulation of *Pdgfa* in BMMCs was pronounced after coculture either with cardiac myocytes or fibroblasts. In our coculture experiments, BMMC-derived PDGF-A accelerated proliferation of cardiac fibroblasts and stimulated synthesis of type III collagen in cardiac fibroblasts. PDGF-A dimeric isoform (PDGF-AA) selectively binds to PDGFR-α (38), and PDGF-AA infusion exerted potent fibrogenic effects, particularly on atrium (Figure 7A), consistent with a previous paper demonstrating that atrial fibroblasts showed higher reactivity to PDGF than ventricular fibroblasts (39). Importantly, the mRNA levels of *Pdgfa* in atrium were significantly increased after TAC operation, which was blunted by depletion of mast cells by BM reconstitution from W/W^v mice. PDGF-A production in atrium is critically relevant to the AF pathogenesis of pressure-overloaded hearts because neutralization of PDGFR-α prevented atrial fibrosis and AF. Collectively, our results suggest that atrial mast cells induce upregulation

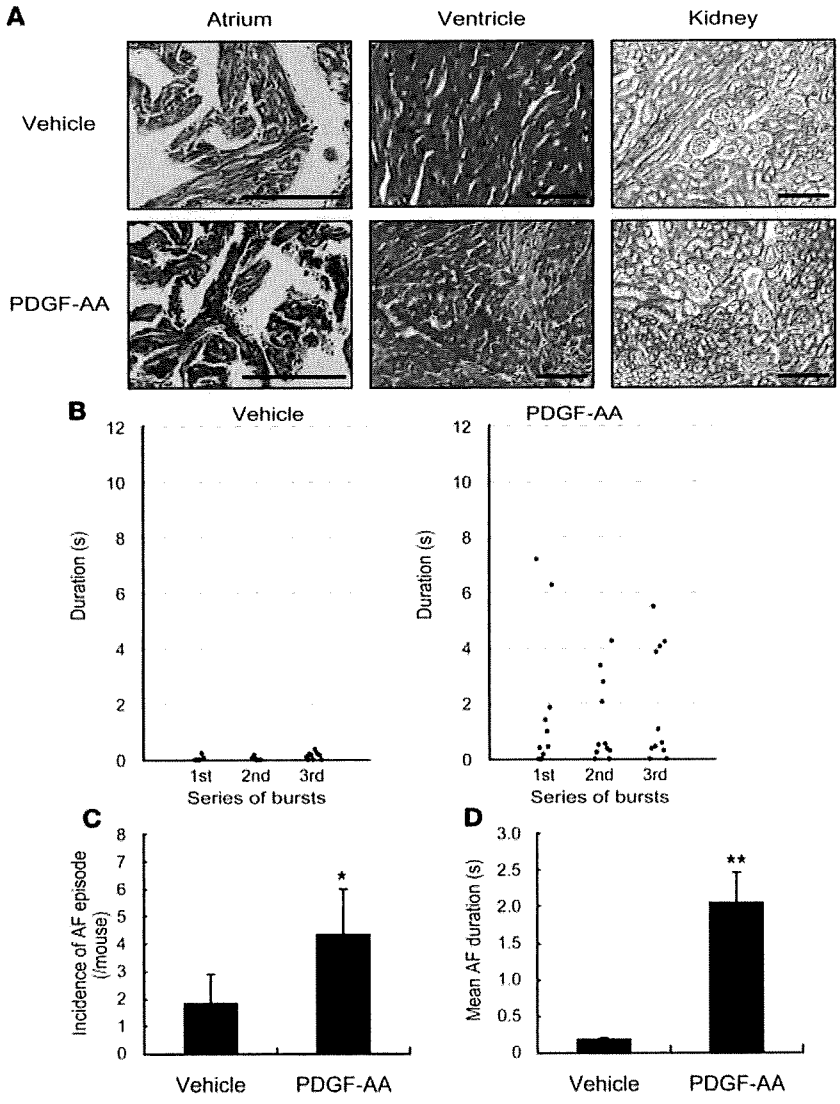

Figure 7
Systemic administration of PDGF-AA induces atrial fibrosis and enhances AF susceptibility in Langendorff-perfused hearts. (**A**) Representative histological sections with Masson's trichrome staining for visualization of fibrosis (blue staining) in the atrium, ventricle, and kidney of mice administered PDGF-AA or vehicle. Scale bars: 20 μm. (**B**) Scatter plot of the duration of AF episodes occurring during 3 series of bursts in mice administered PDGF-AA ($n = 6$) or vehicle ($n = 6$). Duration of AF episodes occurring after each burst are plotted. (**C**) Incidence of AF episodes during 3 series of bursts in mice administered PDGF-AA ($n = 6$) or vehicle ($n = 6$). (**D**) Mean duration of AF episodes during 3 series of bursts in mice administered PDGF-AA ($n = 6$) or vehicle ($n = 6$). Data are presented as mean ± SEM. $^*P < 0.05$ versus vehicle; $^{**}P < 0.01$ versus vehicle.

of *Pdgfa*, leading to progression of a susceptible AF substrate in pressure-overloaded hearts. At present, it remains uncertain whether atrial mast cells are the sole source of PDGF-A. Indeed, mast cell activation can influence the function of many different cell types (12, 24), and especially, macrophages may serve as a source of PDGF-A (38). Further studies using an intricate genetic model to delete *Pdgfa* specifically in mast cells will be required to dissect the importance of mast cell–derived PDGF-A in the pathogenesis of AF.

Several clinical studies have proved the efficacy of pharmacological inhibition of the renin-angiotensin system in the prevention of atrial fibrosis and promotion of AF (40). The therapeutic approach to attenuating or reversing the AF substrate is appealing. Our study highlighted the pathogenic role of mast cells in promoting the AF substrate in pressure-overloaded hearts. Of course, this observation must be further investigated in future studies using large animal models for testing applicability to clinical conditions because variability among species and experimental models may give rise to differences in anatomical and electrophysiological parameters (41). As a starting point for investigations, we propose that the mast cell–PDGF-A axis will be a promising therapeutic target for the upstream prevention of AF in stressed hearts.

Methods

Mice, TAC operation, and echocardiography. All of the experimental protocols were approved by the Institutional Animal Care and Use Committee of Chiba University. C57BL/6 mice, mast cell–deficient W/W^v mice, and congenic +/+ littermates were purchased from Japan SLC. For TAC operation, 10-week-old male mice were anesthetized by i.p. injection of pentobarbital, and respiration was artificially controlled with a tidal volume of 0.2 ml and a respiratory rate of 110 breaths/min. The transverse aorta was constricted with 7-0 nylon strings by ligating the aorta with splinting a blunted 27-gauge needle, which was removed after the ligation. After aortic constriction, the chest was closed and mice were allowed to recover from anesthesia. We confirmed that the magnitude of initial pressure elevation after aortic banding was identical in all groups of mice. The surgeon had no information about the mice used in this study. For evaluation of cardiac dimensions and contractility, transthoracic echocardiography was performed on conscious mice with the Vevo 770 Imaging System using a 25-MHz linear probe (Visual Sonics).

Table 3
Echocardiographic measurements in TAC-APA5 or TAC-IgG mice

	TAC-IgG	TAC-APA5
Number	10	10
HW/BW (mg/g)	5.71 ± 0.18	5.67 ± 0.16
HR (bpm)	633.30 ± 16.06	657.00 ± 11.91
LVDd (mm)	3.54 ± 0.09	3.59 ± 0.08
LVDs (mm)	2.07 ± 0.09	2.01 ± 0.09
FS (%)	41.7 ± 1.48	44.2 ± 1.51
LVPWth (mm)	0.84 ± 0.01	0.81 ± 0.01

Mast cell stabilization and BM reconstitution. For stabilization of mast cells, cromolyn (50 mg/kg/day; Sigma-Aldrich) or vehicle was administrated daily to mice by i.p. injection (14) for the duration of the experiment (10 days after TAC operation). For BM reconstitution, BM cell suspensions were harvested by flushing the femurs and tibias of 8-week-old W/W^v or +/+ mice. The 5-week-old C57BL/6 mice were preconditioned with total body irradiation (9.5 Gy) 6 hours before transplantation. BM cell suspensions (1.0×10^7 cells per mouse) were transfused via the tail vein to the preconditioned recipient mice. The recipient mice were subjected to BM reconstitution for 6 weeks and were subjected to TAC operation.

Induction of AF in ex vivo and in vivo hearts. For induction of AF in ex vivo hearts, hearts were rapidly excised after i.p. injection of heparin (0.5 U/g) and urethane (2 mg/g) and immediately mounted onto a Langendorff perfusion apparatus (42). The hearts were perfused with a nonrecirculating Krebs-Henseleit buffer (119 mM NaCl, 4.8 mM KCl, 1.2 mM KH_2PO_4, 1.2 mM $MgSO_4$, 2.5 mM $CaCl_2$, 10 mM glucose, and 24.9 mM $NaHCO_3$), which was equilibrated with 5% CO_2/95% O_2 at 37°C. All isolated hearts were stabilized for 5 minutes by perfusion at constant flow (3.0 ± 0.2 ml/min) before programmed electrical stimulation. The whole system temperature was kept at 37°C. Two chlorinated silver wires were placed on the base of the heart as indifferent and common ground electrodes. A pair of recording electrodes were placed on the apex and anterior wall of the heart to record ventricular electrograms. Bipolar stimulating electrodes were pressed against the right atrium surface, and bipolar recording electrodes were placed on the left atrium surface to record atrial electrograms.

For induction of AF in in vivo hearts, mice were anesthetized with i.p. injection of pentobarbital and supported by artificial ventilation. The body temperature of mice was monitored and kept at 37°C using a heating pad during the experiments. A 2-French catheter electrode (Japan Lifeline) was placed at the esophageal position dorsal to the left atrium. A surface ECG was simultaneously recorded using electrodes in a lead-II configuration.

Inducibility of AF was tested by applying a 2-second burst using the automated stimulator. The first 2-second burst had a cycle length (CL) of 40 ms, decreasing in each successive burst with a 2-microsecond decrement down to a CL of 20 ms. A series of bursts was repeated 3 times after stabilization for 5 minutes. AF duration was defined as the interval between the rapid irregular atrial rhythm triggered after the bursts and the onset of first normal sinus beat.

Histological analysis. Hearts were excised and immediately fixed in 10% neutralized formalin, and they were then embedded in paraffin. Serial sections of atrium at 5 μm were stained with Masson's trichrome for evaluation of fibrosis. We determined mast cell number and morphology with toluidine blue staining (0.1%; Sigma-Aldrich) and rhodamine-avidin staining (1:100; Vector Laboratories) (20, 26). Specificity of mast cell detection was confirmed by staining sections of W/W^v and +/+ mice at the same dilution of the reagent. The total number of mast cells was counted manually and blindly in 3 microscopic sections from each mouse, and the total area was determined using computer-assisted image analysis (ImageJ; http://rsbweb.nih.gov/ij/).

Hydroxyproline assay. We evaluated collagen content in the atrium by quantification of hydroxyproline, as described previously (43). In brief, the atrium was weighed and then hydrolyzed in 6 N HCl at 100°C overnight. Hydrolyzed tissue was neutralized with NaOH, vacuum dried at 50°C, and resuspended in 1 ml of 5 mM HCl. An aliquot of 20 μl hydrolyzed tissue was added to 180 μl of H_2O in a glass tube. Thereafter, we mixed 100 μl of chloramine-T solution (0.14 g chloramine-T, Sigma-Aldrich; 2 ml H_2O, 8 ml hydroxyproline assay buffer) with the diluted hydrolyzed tissue solution. The ingredients of hydroxyproline assay buffer were as follows: 11.4 g sodium acetate anhydrous (Sigma-Aldrich), 7.5 g trisodium citrate dihydrate (Sigma-Aldrich), 40 ml H_2O (pH adjusted to 6.0), and 77 ml isopropanol, bringing the final volume to 200 ml with H_2O. After incubation for 10 minutes at room temperature, 1.25 ml Ehrlich's reagent (6.0 g p-dimethylaminobenzaldehyde [Sigma-Aldrich], 18 ml 60% perchlorate [Fluka], 78 ml isopropanol) was added and mixed. The samples were incubated at 55°C for 20–25 minutes, and the sample absorbance was read at 558 nm. We used *trans*-4-hydroxy-L-proline (Sigma-Aldrich) (ranging from 0 to 4 mg) to draw the standard curve.

Coculture of BMMCs with cardiac myocytes or fibroblasts. The BM cells were harvested from C57BL/6 mice and cultured for 5 weeks in RPMI 1640 medium (GIBCO; Invitrogen) supplemented with 10% FBS (Equitech-Bio), 0.1 mM MEM Non-Essential Amino Acids Solution (GIBCO; Invitrogen), 4 mM L-glutamine, 25 mM HEPES, 1 mM sodium pyruvate, 50 μM β-mercaptoethanol, 100 U/ml penicillin, 100 μg/ml streptomycin, and 30 ng/ml of recombinant murine IL-3 (PeproTech GmbH) at 37°C in 5% CO_2 (44). By 5 weeks in culture, mast cells were enriched to more than 95%, as assessed by the presence of metachromatic granules in toluidine blue–stained cells and by cell-surface expression of FcεRI (Upstate) using flow cytometric analysis. The cardiac myocytes and fibroblasts were prepared from hearts of 1-day-old Wistar rats, as described previously (45). Dissociated cells were preplated onto 10-cm culture dishes for 30 minutes, which permitted preferential attachment of fibroblasts to the bottom of the dish. Nonadherent cardiac myocytes (3.5×10^5 cells/3.5-cm dish) or adherent fibroblasts (2.0×10^6 cells/3.5-cm dish) were plated on 3.5-cm dishes and cultured for 24 hours in medium (DMEM [GIBCO; Invitrogen], supplemented with 10% FBS, 100 U/ml penicillin, and 100 μg/ml streptomycin). The cells were starved under a serum-free condition for 24 hours before initiation of the coculture. BMMCs (5.0×10^6 cells/3.5-cm dish) were placed onto layers of cardiac myocytes or fibroblasts and were continuously cocultured in DMEM without supplementation with FBS. For stabilization of BMMCs in vitro, BMMCs were pretreated with 10^{-5} M cromolyn (Sigma-Aldrich) for 30 minutes before initiation of coculture, and cromolyn treatment was continued throughout the coculture.

Real-time RT-PCR analysis. Total RNA was extracted by using RNeasy Kit (QIAGEN), and single-stranded cDNA was transcribed by using QuantiTect Reverse Transcription Kit (QIAGEN) according to the manufacturer's protocol. We conducted quantitative real-time PCR analysis with the Universal ProbeLibrary Assays (Roche Applied Science) according to the manufacturer's instructions. Amplification conditions were as follows: initial denaturation for 10 minutes at 95°C followed by 45 cycles of 10 seconds at 95°C and 25 seconds at 60°C. Individual PCR products were analyzed by melting-point analysis. The expression level of a gene was normalized relative to that of *Gapdh* by using a comparative Ct method. The primer sequences and universal probe numbers were designed with the ProbeFinder software as follows: *Pdgfa*, 5′-GTGCGACCTCCAACCTGA-3′ and 5′-GGCTCATCTCACCTCACATCT-3′, no. 52; *Pdgfb*, 5′-CGGCCTGTGACTAGAAGTCC-3′ and 5′-GAGCTTGAGGCGTCTTGG-3′, no. 32; *Col3a1*, 5′-TCCCCTG-